Research Paper

Telomere attrition and dysfunction: a potential trigger of the progeroid phenotype in nijmegen breakage syndrome

Raneem Habib[1,2], Ryong Kim[2,3], Heidemarie Neitzel[2], Ilja Demuth[4,5], Krystyna Chrzanowska[6], Eva Seemanova[7], Renaldo Faber[8], Martin Digweed[2], Reinhard Voss[9], Kathrin Jäger[10,11], Karl Sperling[2,*], Michael Walter[10,11,*]

[1]Department of Human Genetics, Ruhr-University Bochum, Bochum, Germany
[2]Institute of Medical and Human Genetics, Charité - Universitätsmedizin Berlin, Berlin, Germany
[3]Institute of Clinical Chemistry, Red-Cross General Hospital, Pyongyang, Democratic People's Republic of Korea
[4]Department of Endocrinology and Metabolism, Charité – Universitätsmedizin Berlin, Corporate Member of Freie Universität Berlin, Humboldt-Universität zu Berlin, Berlin Institute of Health, Germany
[5]Charité - Universitätsmedizin Berlin, BCRT - Berlin Institute of Health Center for Regenerative Therapies, Berlin, Germany
[6]Department of Medical Genetics, The Children's Memorial Health Institute, Warsaw, Poland
[7]Department of Clinical Genetics, Institute of Biology and Medical Genetics, Second Medical School, Charles University, Prague, Czech Republic
[8]Center for Prenatal Medicine, Leipzig, Germany
[9]Integrated Functional Genomics, Interdisciplinary Center for Clinical Research, University of Münster, Münster, Germany
[10]Institute of Clinical Chemistry and Laboratory Medicine, University of Rostock, Rostock, Germany
[11]Institute of Laboratory Medicine, Clinical Chemistry and Pathobiochemistry, Charité – Universitätsmedizin Berlin, Corporate Member of Freie Universität Berlin, Humboldt-Universität zu Berlin, Berlin Institute of Health, Germany
*Co-senior authors

Correspondence to: Michael Walter; **email:** michael.walter@med.uni-rostock.de
Keywords: nijmegen breakage syndrome, telomere-position effect over long distances, alternative lengthening of telomeres, nibrin, DNA repair
Received: January 8, 2020 **Accepted:** May 27, 2020 **Published:** June 20, 2020

ABSTRACT

Background: Nibrin, as part of the NBN/MRE11/RAD50 complex, is mutated in Nijmegen breakage syndrome (NBS), which leads to impaired DNA damage response and lymphoid malignancy.
Results: Telomere length (TL) was markedly reduced in homozygous patients (and comparably so in all chromosomes) by ~40% (qPCR) and was slightly reduced in NBS heterozygotes older than 30 years (~25% in qPCR), in accordance with the respective cancer rates. Humanized cancer-free NBS mice had normal TL. Telomere elongation was inducible by telomerase and/or alternative telomere lengthening but was associated with abnormal expression of telomeric genes involved in aging and/or cell growth. Lymphoblastoid cells from NBS patients with long survival times (>12 years) displayed the shortest telomeres and low caspase 7 activity.
Conclusions: NBS is a secondary telomeropathy. The two-edged sword of telomere attrition enhances the cancer-prone situation in NBS but can also lead to a relatively stable cellular phenotype in tumor survivors. Results suggest a modular model for progeroid syndromes with abnormal expression of telomeric genes as a molecular basis.
Methods: We studied TL and function in 38 homozygous individuals, 27 heterozygotes, one homozygous fetus, six NBS lymphoblastoid cell lines, and humanized NBS mice, all with the same founder *NBN* mutation: c.657_661del5.

INTRODUCTION

Nijmegen breakage syndrome (NBS) was first described in 1981 in two patients in Nijmegen, in the east of the Netherlands [1]. It is characterized by chromosome instability associated with microcephaly, immunodeficiency, hypersensitivity to ionizing irradiation, and a high predisposition to cancer [2–4]. NBS also displays other symptoms of aging such as postnatal growth retardation, decline in mental function, gray hair, telangiectasias and café au lait spots. Nibrin, a DNA double-strand break (DSB) repair protein, is defective [5, 6], and more than 90% of NBS patients are homozygous for a founder mutation: c.657_661del5 [6–8]. Risk of death from lymphoma is elevated ~1000-fold; by the age of 20, more than 40% of patients have developed a malignant disease, predominantly of lymphoid origin. Even heterozygous carriers of the founder mutation have an increased risk of cancer [8]. In some areas of the world, the *NBN* gene became the most important cancer-predisposing gene [7].

Nibrin is part of the nibrin/Mre11/Rad50 (MRN) complex, which is involved in the repair of DNA double strand breaks (DSBs), the processing of DSBs in immune gene rearrangements, and meiotic recombination [9]. The important role of this complex in mediating the ATM-dependent repair of DSBs probably explains the predisposition to cancer and immunodeficiency in NBS. It is unclear, however, why the incidence of cancer is so much higher in NBS than in other genetic instability syndromes. Nibrin is multifunctional and may also play an important role in protecting the telomeres from inappropriate DNA repair. Telomeric DNA is an evolutionarily highly conserved repetitive sequence that plays a crucial role both in cellular senescence and in carcinogenesis. The exact role of the MRN complex and nibrin in particular in telomere homeostasis is not clear, even though there have been some groundbreaking experimental findings in recent years pointing to a key function in the response to dysfunctional telomeres [10, 11]. Unlike in *S. cerevisiae*, mammalian MRN is not required for association of telomerase to short telomeres [12]. However, experimental *in vitro* and animal data suggest that the MRN complex is required for activation of the ATM-dependent repair of dysfunctional telomeres, the resection of telomeric DNA to create the single-stranded 3' overhang and for stabilization of telomeric T-loops, which is required for telomere replication and elongation [13, 14]. Telomeres recruit Mre11, phosphorylated nibrin, and ATM, which is important for protection and repair of telomeres [15, 16]. The MRN complex protects the leading-strand ends from non-homologous end joining (NHEJ) [17], whereby the telomeres seem to recruit Mre11, phosphorylated nibrin and ATM in every G2 phase of the cell cycle and thus promote the formation of a chromosome end protection complex and a localized DNA damage response [18]. It was proposed that nibrin is required for the proper assembly of the MRN complex, which includes ubiquitination of nibrin upon DSBs [19] and may indirectly influence ATM activation by Mre11 and Rad50 [20].

We therefore hypothesized that NBS is a telomeropathy [21, 22], and that telomere abnormalities may accelerate cancer manifestation. Shorter telomeres have been described in individual NBS cases, for both NBS lymphocytes [23, 24] and fibroblasts [25]. Nonetheless, a systematic investigation has not yet been carried out, and the importance of MRN in general and nibrin in particular for telomere length and function are unclear.

RESULTS

Telomere lengths in human NBS cells and in humanized NBS mice

Relative leukocyte TLs of blood DNA from 38 NBS homozygotes, 27 heterozygotes, and 108 control individuals were measured by qPCR. The mean relative TL of NBS-homozygotes was ~40% shorter in two age-matched groups (1-10 and 11-20 years) than in the control group ($p<0.05$). We found mildly (~25%) reduced TLs in older NBS heterozygotes (>30 years old; $p=0.1$) but not in younger heterozygotes (Figure 1 and Supplementary Tables 1–3).

For Q-FISH analysis, six NBS lymphoblastoid cell lines derived from three individuals with extremely short survival after cancer manifestation (<3 years), and from three individuals with remarkably long survival (>12 years) were analyzed. All six lymphoblastoid cell lines had TLs that were markedly reduced (by ~60-75%) relative to healthy controls ($p<0.05$). Rather short telomeres were found on chromosomes 17, 19, and 20, but this pattern is also a characteristic of normal diploid cells [26], and no preferred shortening of a particular chromosome was observed (Figures 2 and 3).

A positive correlation was found between the TL measured by Q-FISH and the TL measured by qPCR ($r=0.96$); (Supplementary Figure 1). Regression analysis was applied to transform the qPCR data into absolute TLs. In the formula $y=3.4(X)+10.11$, y represents the predicted TRF (Terminal Restriction Fragment) value in kb, X represents the qPCR (T/S) value. The qPCR data and the TRF values showed a moderate correlation ($r=0.64$; Supplementary Figure 2).

A rather uniform TL distribution has been described for most fetal tissues of healthy individuals [27]. In

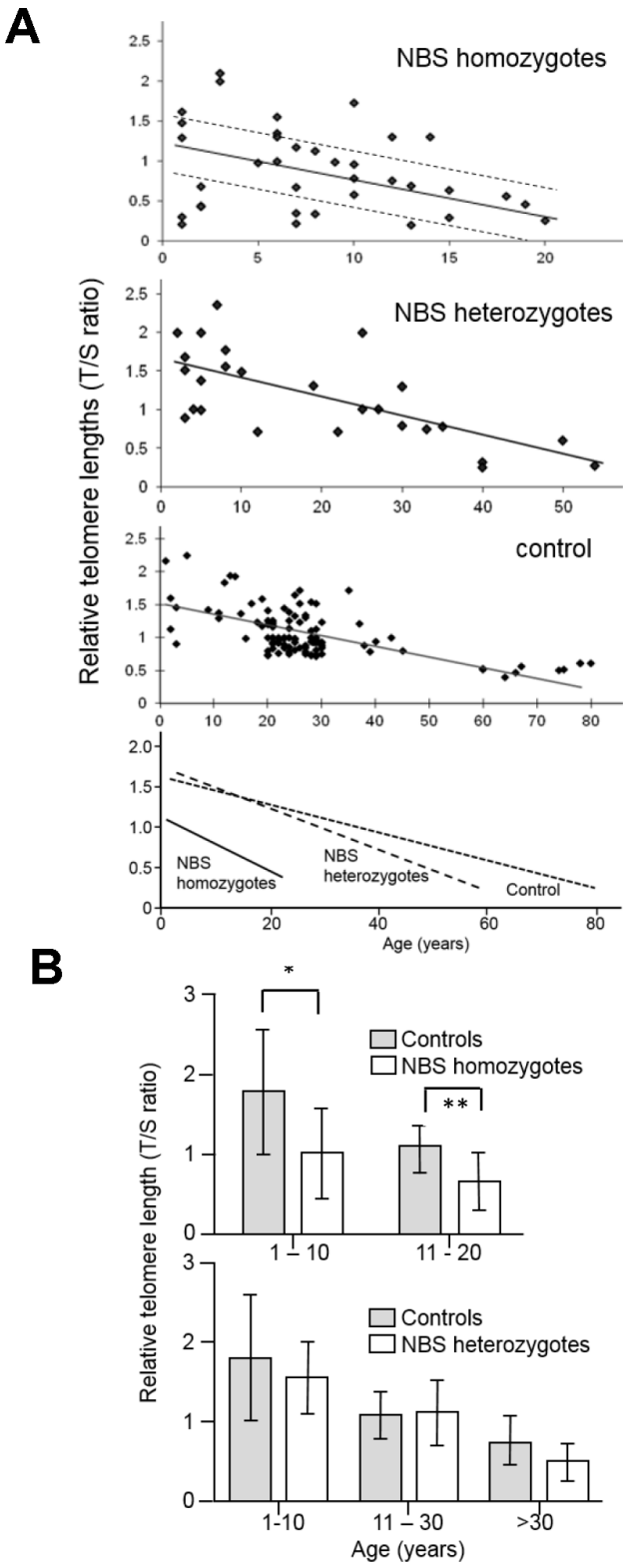

Figure 1. (**A**) Relative telomere length (TL) as a function of age in NBS homozygotes, heterozygotes, and control individuals. Relative TL (T/S ratio) was analyzed from blood samples of 38 NBS homozygotes, 27 NBS heterozygotes, and 108 control individuals by quantitative polymerase chain reaction (qPCR). The dashed lines separate the NBS homozygotes in those with long, medium, and short TL. Below: regression curves standardized for age. Original after thesis Raneem Habib [28]. (**B**) Comparison of TL, as analyzed by qPCR, of NBS homozygotes, heterozygotes, and controls. The comparison was made for age-matched groups (mean values and standard deviation). * indicates $p<0.01$; ** indicates $p<0.001$.

contrast, we found considerable differences in TLs between different fetal tissues: spinal cord and brain tissues had the longest telomeres, while fibroblasts and skin had the shortest, suggesting substantial telomere attrition in these tissues before birth (Figure 4B).

The common human NBN mutation c.657_661del5 is hypomorphic, allowing low-level, functionally relevant, truncated nibrin protein to be formed through an alternative initiation of translation. This is relevant because a loss of function leads to early embryonic lethality in mice [29]. Nbn-/- mice with the human NBS allele display most of the human NBS characteristics with one exception: humanized NBS mice are not prone to early tumorigenesis [29]. The humanized mice analyzed in this investigation expressed the human *NBN* gene, generated by the introduction of the human allele including the 5 bp deletion into *Nbn*-deficient mice ($Nbn^{-/-}NBN^{del5}$). The T/S ratio of control and *Nbn*-deficient mice showed some variability but we did not find significant differences in the TLs between the mice with the NBN founder mutation and the mice with the wild type allele (Figure 4A).

Genetic instability in human NBS cells

The NBS cell lines exhibited spontaneous aberrations, such as chromatid breaks and translocations, as previously described [1–6]. The NBS cell lines in this study displayed a markedly increased rate of chromatid breaks after irradiation (Supplementary Table 4). In one cell line (94P0307) we did find telomere fusions that had not been described in previous NBS studies. All individual telomeres of this line were shorter than those of the control line 06P0131 with one exception: the telomere of the p arm of one chromosome 19, which

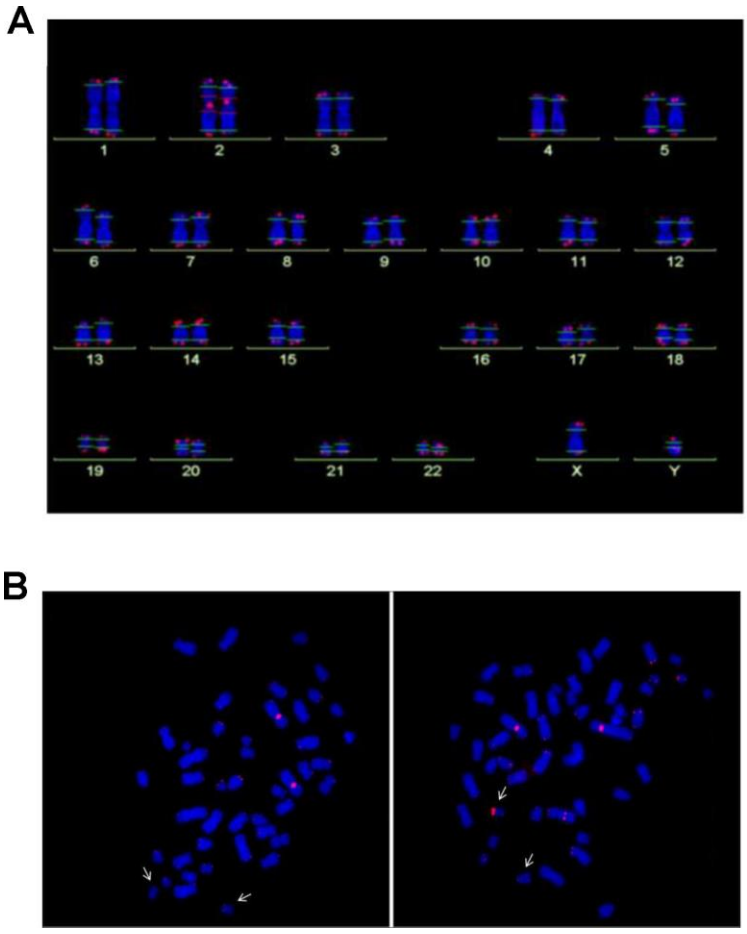

Figure 2. (**A**) Analysis of telomere length by Q-FISH. Normal karyogram with single telomeres stained for telomere repeats (Q-FISH) and a repetitive region in the centromeric region of chromosome 2. The horizontal lines overlaid on each chromosome define the measurement areas. (**B**) Metaphases of the NBS LCL 94P0307 after Q-FISH of the NBS cell line 94P0307 with very short telomeres and a telomere fusion. The arrows point to chromosomes 19. Left panel, Metaphase with weak telomerice fluorescence of both chromosomes 19; Right panel, Metaphase with one chromosome 19 with a brightly fluorescent telomere of the p-arm. The other bright signal is the reference region of chromosome 2. Original after thesis Raneem Habib [28].

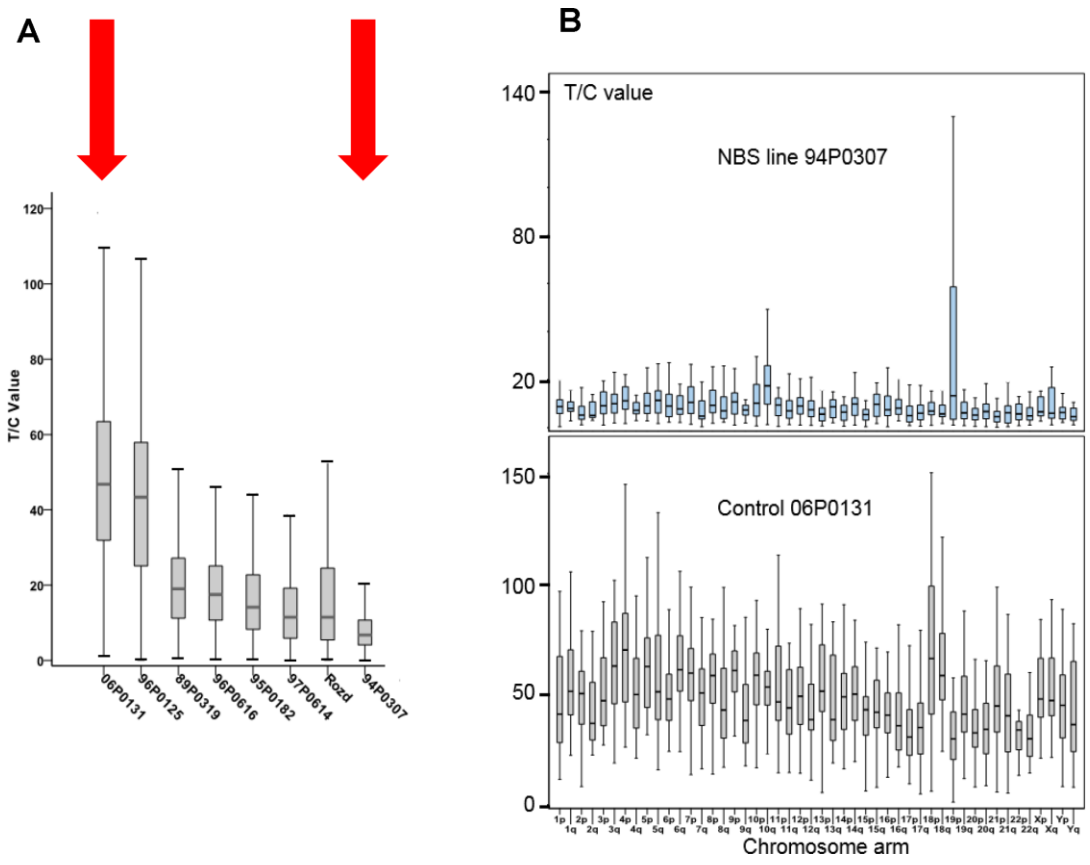

Figure 3. (**A**) Total telomere length (TL) analysed by Q-FISH. TL of six NBS lymphoblastoid cell lines and two control lines (06P0131 and 96P0125) was analyzed by Q-FISH. The boxplot presents the median, the minimum and the maximum T/C values. (**B**) Individual TLs of the NBS line 94P0307 and the control line 06P0131 (red arrows in Figure 3A) analyzed by Q-FISH of 15 metaphases. The boxplot presents the median, the minimum and maximum T/C values. Note the huge variability in TL of the short arm of one chromosome 19 (19p). Original after thesis Raneem Habib [28].

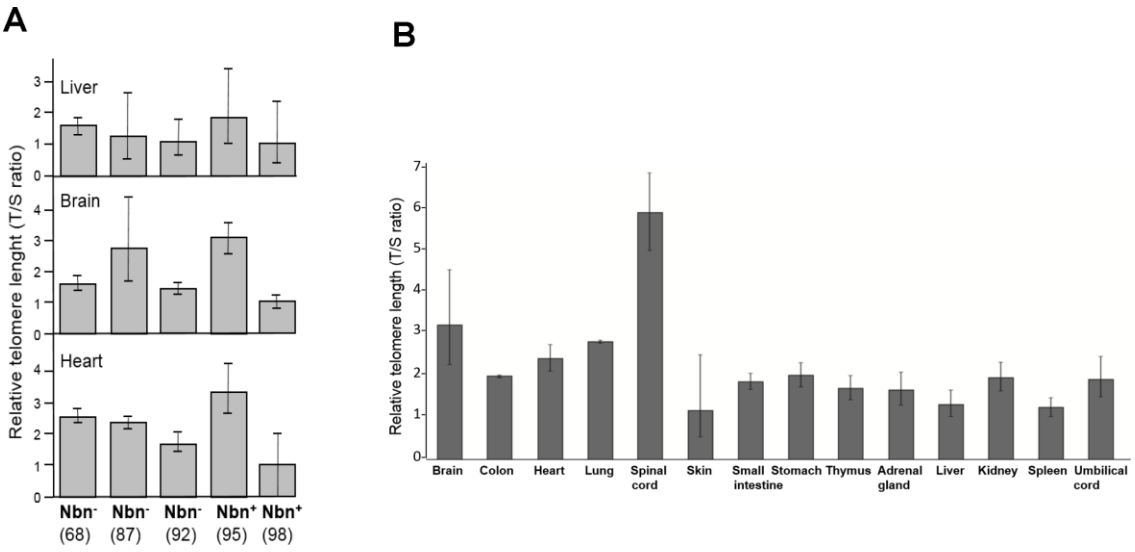

Figure 4. (**A**) Relative telomere length (TL) of three tissues of humanized Nbs mice as estimated by qPCR. Relative TL (T/S ratio) in brain, heart, and liver tissues of humanized Nbs mice (*Nbn*$^{-/-}$*NBN*^{del}, in the figure labelled Nbn^{-}) 87, 68 and 92 (age: 32, 41, and 39 days) and humanized wild-type mice (*Nbn*$^{-/-}$*NBN*$^{+}$, in the figure labelled Nbn^{+}): 95 and 98 (age: 32 days) estimated by qPCR. (**B**) Relative TL of an NBS fetus. Relative TL ±SD (T/S ratio) in 14 different tissues of a 32 week old NBS-fetus estimated by qPCR. Original from [28].

showed an enormous variability in length (Figure 2B; Figure 3 and Supplementary Table 5), due to cellular mosaicism. This telomere was brightly fluorescent in approximately 70% of the metaphases with decreasing tendency during cultivation. The difference in relative T/C values was approximately 11:1 for the two chromosomes 19 (Supplementary Table 6). The expression of *hTERT* was weak in this and all other lymphoblastoid lines analyzed, close to the lower detection limit (Supplementary Figure 3), pointing to alternative lengthening of telomeres (ALT) as the most likely mechanism of telomere elongation in this cell line. Telomere dysfunction–driven genome damage associated with chromosomal break-fusion-bridge cycles and double-strand breaks are frequent in ALT cell lines [30]. In this context, we were interested that the cell line 94P0307 had twice as many aberrations (chromatid breaks and translocations) compared to the other two cell lines with long survival (Supplementary Table 4 and Supplementary Figure 4).

Abnormal regulation of telomeric genes in NBS cells

We investigated possible functional consequences of telomere elongation on 19p and of the expression of telomeric genes *per se*. Telomeres may loop to specific loci to regulate gene expression; this process is called TPE-OLD (telomere position effect over long distances) [31]. Individual genes or gene regulators close to the telomeres are silenced in young cells (with long telomeres) and become expressed when telomeres are short. Re-elongation of short telomeres in cells by exogenous expression of the *hTERT* gene (active telomerase) normally results in reorganization of functional telomeres and expression patterns similar to those in young cells with long telomeres, up to 10-15 Mbp away from the telomere [31]. We were interested to know if long 19p telomeres might influence the mRNA expression of telomeric genes. Using Affymetrix cDNA microarray analyses and fibroblasts from healthy volunteers and Hutchinson Gilford progeria (HGP) patients we identified ten genes on 19p that were differentially regulated at the level of mRNA in pre-senescent cells (with short telomeres) and in *hTERT* immortalized cells (with long telomeres) and that were not differentially regulated by UV-B irradiation as a model for stress-induced senescence (Supplementary Table 7 and Supplementary Figures 5–8).

As shown in Figure 5 and Supplementary Table 8, differential regulation in array experiments was confirmed by qPCR for all ten genes in the healthy control fibroblasts. The extremely elongated telomere of 19p in the lymphoblastoid cell line did not show any suppressive or enhancing effect on mRNA level (Figure 5). By contrast, the expression of all TPE-OLD candidate genes was markedly altered in pre-senescent NBS fibroblasts. We observed lower mRNA levels for *BSG* (-61%), *GAMT* (-35%), *SCAMP4* (-52%), *OLFM2* (-90%). *COL5A3* (-92%), *CACNA1A* (-91%) and *NOTCH 3* (-42%), and we observed increases for *UHRF1* (12.5-fold), *RNASEH2A* (15.1-fold), and *DDX39A (3.8*-fold*)* in pre-senescent NBS compared to pre-senescent control fibroblasts. The telomere-dependent regulation was even reversed for *UHRF1, RNASEH2A*, *CACNA1A* and *DDX39A*. All TPE-OLD candidates encode proteins involved in senescence or cell growth. *BSG* encodes the metalloproteinase EMMPRIN that may trigger matrix metalloprotease and cytokine production and plays an important role in heart remodeling in aging mice [32]. The *GAMT* gene product guanidinoacetate methyltransferase catalyzes creatine synthesis, which may help to replenish cellular ATP [33], possibly for senescence-associated secretory phenotype (SASP) [34]. *SCAMP4* gene product secretory carrier membrane protein is a direct player in SASP [35]. The *OLFM2* gene product olfactomedin 2 is an age-dependent regulator of cell differentiation and regulates axonal growth [36]. *COL5A3* induces collagen synthesis and is involved in age-dependent tissue remodeling [37]. *CACNA1A* regulates calcium entry age-dependently and plays a role in neurodegeneration [38]. *NOTCH3* functions as a tumor suppressor by controlling p21-mediated cellular senescence [39]. By contrast, *UHRF1* is a negative regulator of senescence. Cellular senescence can be induced by phosphorylation and inactivation of UHRF1 [40]. *RNASEH2A* enhances migration and invasion and may play a role in cancerogenesis [41]. *DDX39A* is a RNA helicase and Telomeric Repeat Factor 2 (TRF2)-interacting protein with suspected roles in both cancer and longevity [42]. Altogether, these data suggest abnormal regulation of telomeric aging genes in NBS cells.

Relationship between telomeres length, disease progression, and cell pathology

There was no significant correlation between the TL and either the age at cancer manifestation or age at death (Table 1, Supplementary Table 9). This result was surprising insofar as we expected a worse phenotype in patients with short telomeres. Thus we explored the possibility that short telomeres may have stabilized the phenotype in a senescence-like state in all or in individual patients. To test this possibility, we measured caspase 7 activity as a surrogate marker for apoptosis. Senescent fibroblasts resist apoptosis by downregulating caspases. As shown in Table 2, caspase activity was significantly higher in the three cell lines derived from patients with shorter survival and longer telomeres compared to those with longer survival and shorter telomeres (2.8-fold; $P<0.05$, 48h after 10 mg/ml

bleomycin). The cell line 94P0307 with the shortest telomeres displayed an extremely low (almost undetectable) caspase activity. Moreover, the cell lines derived from patients with shorter survival displayed on average twice as many chromatid breaks as the cells from patients with long survival (Supplementary Table 4). Altogether these data point to a more stable phenotype with a higher "degree" of senescence in cells from patients with long survival.

There is a close functional link between ATM and nibrin [43]. As shown in Table 2, the radiomimetic bleomycin induction of ATM-Ser 1981 phosphorylation was not significantly different among cell lines with

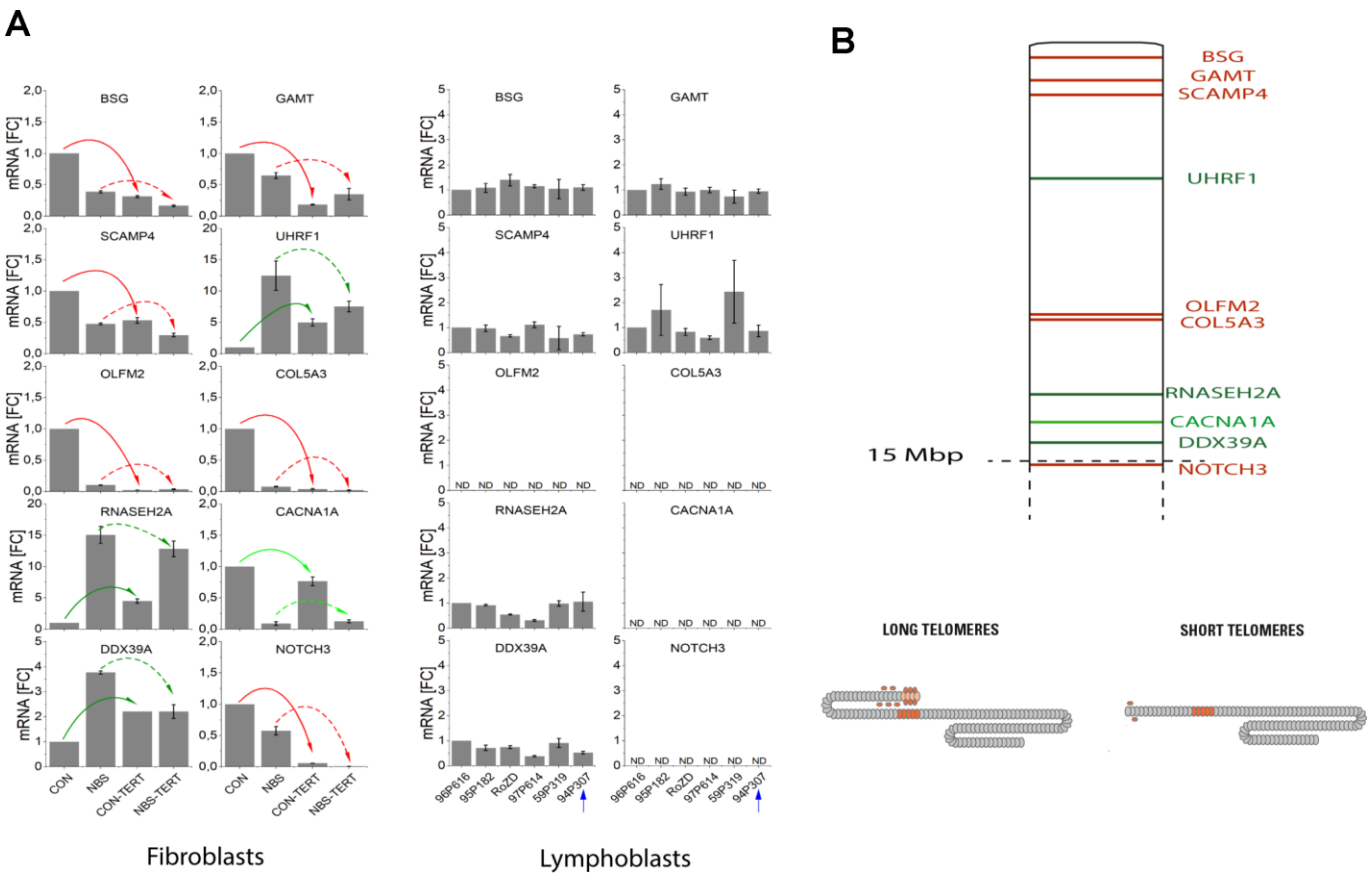

Figure 5. (**A**) mRNA expression of TPE-OLD candidate genes in cells with normal/short telomeres and artificially elongated telomeres in the presence of hTERT. qPCR analysis was performed in a healthy human fibroblast cell line, a NBS fibroblast cell line, and in all 6 available lymphoblastoid cell lines (LCLs). Total mRNA was extracted from proliferating fibroblasts and from the same cell lines proliferating with experimentally elongated telomeres, after immortalization with *hTERT*. In LCLs, mRNA from the 6 different donors was compared. One of these cell lines (94P307) showed extremely elongated telomeres on p19. The genes were identified as TPE-OLD candidates by use of Affymetrix gene chip experiments in independent cell lines from healthy controls and HGP patients (as described in Supplementary Tables 7–8 and Supplementary Figures 5–8). All values were normalized to the level (=1-fold) of mRNA in unmodified and pre-senescent control fibroblasts. Each assay was performed in triplicate. Red arrows mark the genes with attenuated regulation in NBS (short telomeres in pre-senescent vs. long telomeres in *hTERT* infected cells). Green arrows mark the genes with reversed regulation in NBS (dark green: downregulated in pre-senescence in controls; light green upregulated). The blue arrow marks the LCL with extremely long telomeres on 19p. *BSG*: basigin; *GAMT*: guanidinoacetate methyl-transferase; *SCAMP4*: secretory carrier membrane protein 4; *OLFM1*: olfactomedin 1; *UHRF1*: ubiquitin like with PHD and ring finger domains 1; *COL5A3*: collagen type V alpha 3 chain; *RNASEH2A*: ribonuclease H2 subunit A; *CACNA1A*: calcium voltage-gated channel subunit alpha1 A; *DDX39A*: DExD-box helicase 39A; *NOTCH3*: Notch receptor 3. ND, non detectable (mRNA quantifications with Ct values above 35). Borderline Ct values were detected for NOTCH3 for the LCL 95P182 (mean Ct = 34.9) and 59P319 (mean Ct = 34.6), not shown in the figure. (**B**) TPE-OLD concept. Telomeres loop to specific loci to regulate gene expression, a process termed telomere position effect over long distance [31]. The effect may likely extend to a distance of at least 10-15 Mbp from the telomere. The marked TPE-OLD gene candidates on 19p were investigated in experiments shown in Figure 5A: *BSG*, *GAMT*, *SCAMP4*, *OLFM2*, *COL5A3*, *CACNA1A*, *NOTCH3* (upregulated in pre-senescent cells), and *UHRF1*, *DDX39A* and *RNASEH2A* (downregulated in senescent cells). TPE-OLD genes may form clusters with reverse regulation in NBS (green) further away from the telomere.

Table 1. Relationship of telomere length of NBS homozygotes with age at cancer manifestation and age at death.

Telomere length	Origin	ID/DNA	Cancer	Ig Status	Age at cancer manifest.	Mean ± SD	Age at death	Mean ± SD
	Po	94P629	B-NHL	IgA+IgG↓	9		9	
	Po	97P614	B-NHL	normal	7		19	
			DLBCL-1		11			
			DLCBL-5		27			
	Po	8294	T-NHL	unknown	14		16	
	Po	98P222	Pre-B-ALL	unknown	5		6	
	Ge	94P126	NHL	unknown	13?		19?	
	Po	97P081	T-NHL	IgA+IgG↓	24		24	
	Po	94P251	HL	IgA+IgG↓	12		14	
	Po	94P548		IgA+IgG↓			8	
	Po	5567	T-NHL	unknown	34		34	
	Po	96P551		normal				
	Cz	5431	NHL	unknown	24		29	
	Cz	7822	NHL	unknown	7		10	
					6			
					17			
	Po	96P473		IgA+IgG↓				
	Po	97P229	B-NHL	IgA+IgG↓	4		6	
	Po	97P751	Cause of death unclear	unknown			3	
	Po	95P185		IgA+IgG↓				
	Po	95P182	B-NHL	IgA+IgG↓	8		10	
	Po	94P195	T-NHL Precursor TLBL	normal	19		21	
	Po	94P192	TLBL/ALL?	IgG↓	35		36	

*Age-adjusted Po, Poland; Ge, Germany; Cz, Czech Republic.

Table 2. Analysis of caspase-7 and ATM phosphorylation after bleomycin treatment of six NBS lymphoblastoid cell lines with the absolute longest (above) and absolute shortest (below) telomere lengths.

	Survival (y)	Caspase-7 activity after bleomycin treatment (10 µg/ml)				pATM/ATM level after bleomycin (1h)		
		0h	12h	24h	48h	0 µg/ml	10 µg/ml	30 µg/ml
89P0319 ♀	0	0.65±0.26	0.77±0.22	0.78±0.17	0.90±0.13	0,17±0,05	0,56±0,01	0,74±0,03
96P0616 ♀	0,2	0.17±0.01	0.24±0.01	0.41±0.05	0.90±0.08	0,07±0,05	0,24±0,06	0,47±0,06
95P0182 ♀	2,8	0.17±0.14	0.25±0.15	0.46±0.11	0.65±0.10	0,04±0,03	0,28±0,07	0,53±0,06
		0.33±0.28	**0.42±0.30**	**0.55±0.20**	**0.82±0.14**	**0,09±0,07**	**0,36±0,17**	**0,58±0,14**
97P0614 ♂	>12	0.13±0.03	0.16±0.05	0.36±0.09	0.49±0.05	0,04±0,02	0,16±0,07	0,22±0,08
RoZd ♀	>12	0.13±0.08	0.15±0.01	0.27±0.01	0.36±0.05	0,06±0,05	0,30±0,09	0,39±0,04
94P0307 ♂	>12	0.01±0.01	0.02±0.01	0.02±0.01	0.03±0.02	0,11±0,08	0,29±0,06	0,45±0,02
		0.09±0.07	**0.11±0.08**	**0.22±0.18**	**0.29±0.24**	**0,07±0,04**	**0,25±0,08**	**0,35±0,12**
		P=0.22	P=0.16	P=0.09	**P=0.03**	P=0.62	P=0.38	P=0.10

Each experiment was repeated three times; Mean ± SD.

short or long survival rates. Also, the cell line with low caspase 7 activity had normal ATM function.

DISCUSSION

Accelerated telomere attrition and telomere dysfunction in NBS cells

The main finding of this work is the stronger than expected telomere shortening and functional restriction in NBS patients. NBS homozygotes showed significantly shorter TL in all age groups. TL was reduced in homozygous patients by ~40% (qPCR). TL was ~25% shorter in NBS heterozygotes older than 30 years. The latter result was borderline significant (p=0.1) but remarkable in view of the lower age in NBS heterozygotes (42 y vs. 57 y in controls). Even stronger differences in TL were observed with qFISH (60-70%) in a subset of six homozygous NBS patients.

The variability of TL depending on the method suggests that telomeric and subtelomeric sequences are affected. We found only a moderate correlation between qPCR and TRF values, which is plausible insofar as the localization of the subtelomeric region included in the measurement is variable in TRF analysis based on the restriction enzymes used. Similar observations (with comparable correlation coefficients) have been made in other studies [44]. The advantage of the TRF method is the measurement of TL in absolute values (bases); on the other hand there is the disadvantage of being dependent on restriction enzymes with interindividual and intersexual biases [45]. Using qFISH rather short telomeres were found on chromosomes 17, 19, and 20. Yet this pattern was very similar to that of normal diploid cells [26].

In one NBS lymphoblastoid cell line (94P0307), we found striking telomere fusions with extreme telomere elongation in cells with very low *hTERT* expression. There is evidence that in humans the *hTERT* gene is close to the telomere and influenced by TPE-OLD [46]. However, silencing of *hTERT* in this cell line is unlikely because the *hTERT* gene is located on chromosome 5p and the extremely elongated telomere is located on chromosome 19p. We did not search for c-circles and ALT-associated promyelocytic leukemia protein (PML) bodies in this investigation. However, we had some indirect evidence for possible ALT involvement. Telomere dysfunction–driven genome damage associated with chromosomal break-fusion-bridge cycles and double-strand breaks are frequent in ALT cell lines [30], and were also observed in this cell line. This is remarkable insofar as ALT normally requires the activity of the Mre11/Rad50/nibrin recombination complex [14, 47, 48]. However, there are several ALT mechanisms [14], and ALT may have occurred by homologous recombination and telomere-sister chromatid exchange [14]. Altogether, these *in vitro* experiments are consistent with both the proposed function of nibrin in telomere protection [18–20] and with the occurrence of cancer forms with high ALT prevalence in NBS [49].

Telomere extension was possible with telomerase in cultivated control and NBS fibroblasts. We were able to find expected changes on mRNA levels in control fibroblasts for all TPE-OLD candidate genes investigated on 19p. But we did not find expression changes of telomeric genes for the lymphoblastoid cells with abnormal 19p elongation; the TL-dependent regulation of the genes *BSG, GAMT, SCAMP4, OLFM2, COL5A3,* and *NOTCH 3* was attenuated in NBS fibroblasts, and it was reversed for the genes *UHRF1, RNASEH2A, CACNA1A* and *DDX39A*. These data show that NBS cells are still capable of elongating telomeres. Yet functionally abnormal telomeres may arise.

Possible causes for accelerated telomere attrition in NBS cells

The NBN mutation c.657_661del5 may affect a variety of functions leading to disturbed telomere repair and accelerated telomere attrition. The MRN complex is required for activation of the ATM-dependent repair of dysfunctional telomeres, the resection of telomeric DNA to create the single-stranded 3’ overhang and for stabilization of telomeric T-loops [13, 14]. The Mre11-nibrin interaction required for ATM activation [20] may be affected as well as nibrin ubiquitination [19] and/or phosphorylation [18], which is important for cell cycle dependent telomere conservation and repair [18]. In accordance with current concepts (with nibrin as a co-factor for MRN complex assembly and a more indirect activation of ATM [18–20]) ATM phosphorylation was not impaired in our experiments, which does not point to a direct functional interference with ATM activation.

Increased oxidative stress has previously been described for NBS cells [50, 51]. The observation that G:C>A:T is the most frequent spontaneous base mutation in NBS [52] is of interest insofar as the telomeric TTAGGG sequence is sensitive to oxidative modifications and single-strand breaks [53]. Thus a high vulnerability of telomeres to oxidative damage may contribute to accelerated telomere attrition. The occurrence of ALT cells, and persistent DNA replication stress may additionally lead to spontaneous mitotic telomere synthesis, a potential driver of genomic duplications in cancer [14]. Our findings in fetal tissue suggest that substantial TL attrition may occur before birth in NBS

homozygotes, which cannot be explained by the "end replication problem" alone. There were considerable differences in TLs between different fetal tissues. This is in sharp contrast to observations from healthy fetuses showing a very uniform TL in all tissues at all gestational ages [27].

Possible implications of telomere attrition for cancerogenesis

Genetic instability and impaired telomeric repair may synergize with telomere attrition and dysfunction to explain the extremely high cancer incidence in NBS. The "dose dependency" of telomere attrition on the phenotype also account for this possibility. Homozygote NBS patients with marked telomere attrition develop cancer at young age. Heterozygote patients have an increased cancer risk at higher age, and humanized NBS mice with normal TL did not display early tumorigenesis, but showed all other signs of NBS [29]. The higher TL reserve in mice [53, 54] may explain why we observed no significant reduction in TL in the NBS mice. Overall, these data are consistent with epidemiological studies that have demonstrated a strong inverse relationship between TL and cancer incidence in the general population [55–57].

A possible explanation for the high lymphoma incidence in NBS could be the high rate of somatic recombination with associated hypermutability. This hypermutability is required for the extreme degree of somatic recombination of the immunoglobulin and T-cell receptor genes necessary for the vast repertoire of antibodies and T cell receptors [56]. On the other hand, the almost inevitable development of T or B cell lymphoma during childhood and the extreme preference over other types of cancer is striking. Two key steps are important for tumorigenesis: increased mutation rate and clonal selection with a growth advantage. The unique combination of hypermutability and extreme telomere attrition may have contributed to the high incidence of lymphomas at young age. In this context, it is noteworthy that all suggested TPE-OLD genes on p19 are functionally involved in cell senescence or cell growth and that all these TPE-OLD candidates were dysregulated in the NBS fibroblast cell line. Genes with suggested functions in senescence were suppressed, whereas growth promoting genes were rather increased on mRNA level (Figure 5 and Supplementary Table 8). Even if we had not the opportunity to show this dysregulation in cultivated (Epstein-Barr virus transformed) lymphoblastoid cell lines it is possible that TPE-OLD dysregulation favors a growth advantage *in vivo*, which synergizes with the extreme hypermutability and may explain the dramatically increased risk for developing lymphoma to over 1000-fold in NBS, which was not found in any other disease, including other DNA repair syndromes [56].

Possible implications of telomere attrition for tumor suppression

We did not find an inverse correlation between TL and age of cancer onset. A combination of the TL, the degree of telomere damage, the number of critically short telomeres per cell, and other individual factors may also influence cancer onset. Alternatively, the deleterious effect of TL attrition is to some extent superimposed by some other more beneficial effect. In this context, we found it interesting that individual patients survived their disease for more than a decade. Cultivated lymphoblastoid cells derived from NBS patients with long survival times (>12 years) displayed shorter telomeres and lower caspase 7 activities, compared to cells derived from patients with short survival times (<3 years), suggesting low apoptosis rates and/or increased senescence rates with (at least in these individual patients) effective tumor suppression. The limit on cellular proliferation for cells with short telomeres is considered an initial block to oncogenesis [58]. Data may point to a direct protective effect of short telomeres in these patients.

These results are important to a better understanding of the role of telomere attrition in carcinogenesis *per se*. It is generally accepted that telomere attrition drives genomic instability and that the subsequent acquisition of *hTERT* expression and telomerase activity is involved in cancer immortality [59]. This model is supported by clinical findings showing that short telomeres are an important risk factor for malignant transformation [57]. On the other hand, longer telomeres can be a predictor for poor outcome after a tumor has developed [60]. This, at first glance, contradictory observation is usually attributed to higher telomerase activities (and thus a higher "degree" of immortality) in tumor patients with poor outcome. However, other findings indicate that the activation of telomerase may occur early in tumor development [59, 61]. The exact temporal sequence of telomerase activation, telomere shortening and malignant transformation is not clear. The data presented here illustrate the double-edged sword of telomere shortening in NBN founder mutation carriers with lymphoid malignancies (and thus confirm the current concept) but also show an alternative explanation for the correlation between TL and tumor progression: lower apoptosis and/or increased replicative senescence rates due to short telomeres and thus relative protection against new tumors (summarized in Figure 6). This may have important therapeutic implications. For example,

hematopoietic stem cell transplantation (HSCT) appears to be a promising therapeutic strategy for some but not all NBS patients [62]. From a therapeutic point of view, our data suggest that telomere stabilization should indeed be the goal for NBS (and possibly other tumor) patients *before* cancer onset, but after cancer has already developed, "keeping telomeres short" would probably be more useful. Considering new therapeutic options for influencing telomeres [58] these findings could become clinically relevant for this and other cancer-predisposing mutations with involvement of telomere attrition and/or dysfunction.

Estimating the relative contribution of telomere shortening to cancerogenesis is difficult, especially in view of the bifunctional role of telomere shortening. The DNA repair defect has likely a major contribution to cancerogenesis. According to recent recommendations for a novel nomenclature [21, 22], NBS is clearly a secondary telomeropathy. Our data do not currently warrant the classification of the disease as a classical "impaired telomere maintenance spectrum disorder" (ITM). Secondary telomeropathies include diseases in which it is not clear to what extent the telomere dysfunction is the cause of the pathology.

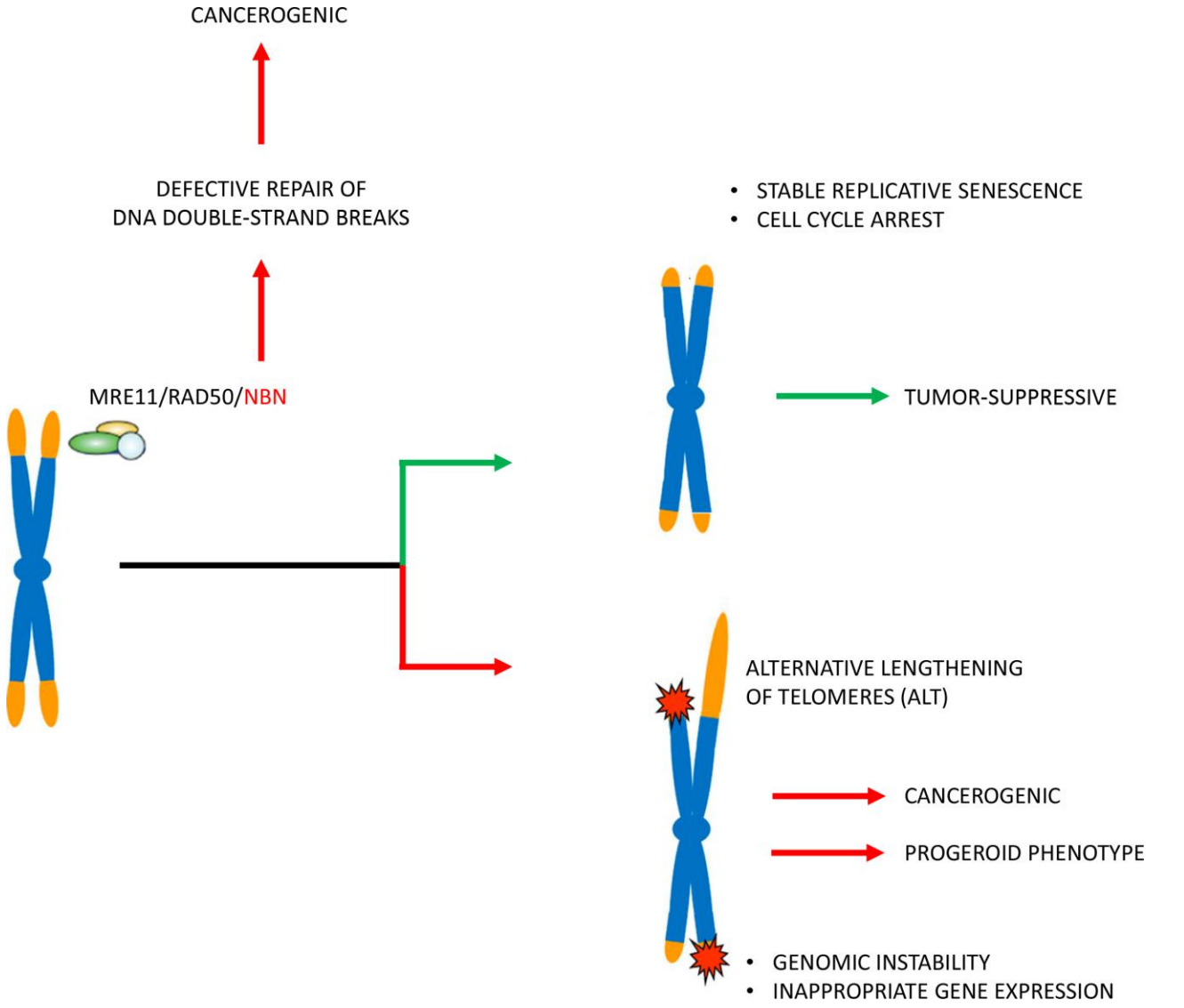

Figure 6. Pathophysiological concept. The patients' cells in Nijmegen Breakage Syndrome have markedly reduced telomere lengths. Telomere attrition may induce genetic instability and alternative telomere elongation and thus enhance the cancerogenic effect (that is induced by defective repair of DNA double-strand breaks by non-homologous end joining) and also contribute to a progeroid phenotype. Telomere attrition may, however, also mitigate the clinical phenotype by inducing stable replicative senescence and cell cycle arrest. The latter is indicated by cells from patients with long tumor survival times with very short telomeres and little apoptosis.

Possible implications of telomere attrition for the progeroid phenotype

NBS belongs to the progeroid syndromes and patients have symptoms of aging such as decline in mental function, gray hair, teleangiectasia and café au lait spots. It has been shown that transient introduction of telomerase mRNA into progeria cells improves many of the hallmarks of this disorder [63]. It is assumed that telomere dysfunction in Hutchinson Gilford progeria and likely other telomere syndromes is a causative molecular mechanism of pathogenesis [64]. The data presented here expand this concept and show that abnormal TPE-OLD may contribute to the progeroid phenotype in NBS. Using independent methods comparing replicative, stress-inducible and *hTERT* immortalized cells, we identified ten TPE-OLD candidate genes with significant TL-dependent expression changes. Seven of the TPE-OLD candidate genes were upregulated in aged healthy fibroblasts and are involved in senescence pathways or have some functional relation to aging. Three of the genes had rather growth promoting function and were suppressed in normal fibroblasts on mRNA level (Figure 5 and Supplementary Table 8). The TL-dependent response was attenuated for all seven upregulated genes in NBS fibroblasts and was reversed in all three growth promoting genes, suggesting that the normal senescence program is disturbed in these cells and shifted to a rather growth promoting expression pattern.

Thus coordinated regulation of telomeric genes could be important for (patho)physiology. We postulate that the progeroid phenotype in NBS is intimately influenced by TPE-OLD. In the age-associated genetic disease facioscapulohumeral muscular dystrophy *SORBS2* transcription is altered by a telomeric 4.8-Mb loop in patients´ myoblasts. *SORBS2* is normally up-regulated by maturation/differentiation of skeletal muscle and is misregulated by TPE-OLD-dependent variegation in myoblasts [65]. NBS is a secondary telomeropathy in which telomere dysregulation occurs at multiple sites. We cannot entirely exclude that some changes on mRNA level occurred secondarily as part of an adaptation mechanism. However, the extremely accelerated telomere attrition is a plausible explanation for abnormal TL-dependent regulation in NBS cells and modulation of the clinical phenotype. A role in pathogenesis is also supported by the significantly milder clinical phenotype in NBS mice with significantly longer telomeres. Humanized NBS mice have less severe immune system defects and are not markedly prone to malignancy.

The pathophysiological role of short telomeres in diseases with short telomeres is mostly attributed to replicative exhaustion, increased DNA damage response, genetic instability and missing scavenger for oxygen radicals. The studies presented here show another mechanism that could be effective independent from DNA damage response and long before the onset of senescence: an imbalance or dysfunction in telomere position effect.

All progeroid syndromes can be classified into two categories: those caused by alterations in components of the nuclear envelope; and those caused by mutations in components of the telomerase complex. Short telomeres have now been described for almost all progeroid syndromes with mutations in genes involved in DNA-repair pathways, including Rothmund-Thomson syndrome, Werner Syndrome, Dyskeratosis congenita, Ataxia teleangiectasia, Ataxia teleangiectasia like syndrome, Bloom syndrome, and NBS [21, 22]. The progeroid syndromes with short telomeres resemble each other in many aspects and short telomeres are a potential cause or co-factor for symptoms such as nail atrophy, alopecia, gray hair, immunodeficiency and possibly also cancerogenesis. George Martin described the progerias as segmental diseases [66] and characterized their pathology and many molecular defects in pioneering investigations (summarized in reference [67]). In his original definition, each disease captures some, but not all, of the symptoms of aging, each with different (segmental) affected organ systems. The data described here support a more modular instead of a strictly segmental model, in which the aging phenotype is caused by a limited number of modules, as originally proposed by Hofer et al. [68], some of which are unique and some of which overlap the symptoms of other modules. TPE-OLD can provide an explanation for this model on a molecular basis. Depending on the degree of the telomere damage and disease-specific peculiarities, a phenotype variety may result with a more progeroid or more cancerogenic gene expression pattern.

MATERIALS AND METHODS

Cell cultures

The fibroblast cell lines were propagated in Amniomax medium with gentamicin sulfate and L-glutamine supplement. Lymphoblastoid cells (LCLs) were prepared and cultured as described [69].

DNA samples

DNA was isolated from the blood of 27 NBS heterozygotes, 38 NBS homozygotes, a homozygous NBS fetus, and 108 controls. The NBS fetus presented with microcephaly, craniofacial dysmorphology, and signs of immaturity, but no malformation of inner organs. The pregnancy was interrupted in the 32nd week.

Molecular genetics

The founder mutation was analyzed as previously described [6]. Expression of the human telomerase reverse transcriptase gene (*hTERT*) was analyzed by qPCR. GAPDH was used as the internal control gene. The primer sequences for *hTERT* were: 5'- CCG ATT GTG AAC ATG GAC TAC GT -3'(forward); 5'- CGT AGT TGA GCA CGC TGA ACA -3'(reverse). The primer sequences for GAPDH were: 5'-CTC TGC TCC TCC TGT TCG AC-3'(forward); 5'-GCG CCC AAT ACG ACC AAA TC-3'(reverse).

mRNA quantification of TPE-OLD (telomere position effect over long distances) candidate genes was carried in triplicates in a 384-well plate using a BioRad CFX384 real-time C1000 thermal cycler, as described [70]. Human PPIA (Cyclophilin A) (Cat. 4333763F) was used as an endogenous control. The ΔΔCt method was used for relative quantification [70]. The following gene expression TaqMan assays (Applied Biosystems) were used: BSG (Cat. Hs00936295_m1), CACNA1A (Cat. Hs01579431_m1), COL5A3 (Cat. Hs01555669_m1), DDX39A (Cat. Hs01124952_g1), GAMT (Cat. Hs00355745_g1), NOTCH3 (Cat. Hs01128537_m1), OLFM2 (Cat. Hs01017934_m1), RNASEH2A (Cat. Hs00197370_m1), SCAMP4 (Cat. Hs00365263_m1), and UHRF1 (Cat. Hs01086727_m1). qPCR was applied to determine the relative telomere length as described previously [71]. The relative length of individual telomeres was analyzed by quantitative fluorescence in situ hybridization (Q-FISH) [72]. The fluorescence intensity of single telomeres *(T)* relative to a constant repetitive region in the centromeric region (C) of chromosome 2 (T/C ratio) was measured, using Ikaros software. The T/C ratio of 15 metaphases was estimated, and the mean telomere intensities of the p-arms and q-arms were calculated for each chromosome.

Absolute TL was measured by Terminal Restriction Fragment (TRF) length analysis, using the Roche - TeloTAGGG TL assay and the restriction enzymes Hinf1 and Rsa1 [28].

Humanized NBS mice, kindly provided by André Nussenzweig, were generated by reconstitution of *Nbn* knockout mice with the human *NBN* gene carrying the c.657_661del5 mutation or the wild type allele [28].

hTERT immortalization

Fibroblasts were infected with retroviral supernatants from a packaging cell line (PA317-TERT) that stably expresses the human telomerase cloned into a pBabePuro vector, as described previously [73].

Identification of TPE-OLD candidate genes in human fibroblasts

Using an Affymetrix cDNA microarray, we compared the expression profiles of pre-senescent fibroblasts and *hTERT* immortalized fibroblasts. As a model for stress-inducible senescence, we used UV-radiated cells (radiated twice per day, for 3 consecutive days, with a total dose of 528 J/m², using four 20W TL/12 lamps emitting broadband UV-B peaking at 312 nm). Senescence was confirmed by β-galactosidase staining. We analyzed 16 microarrays, each with 54,675 transcripts on an HGU133-A2.0 array from Affymetrix®, in a design with 3 groups. Differentially expressed genes in replicative senescence, up to 15 Mbp telomeric on p19, that were not differentially expressed in UV-B treated cells were viewed as potential TPE-OLD candidates.

Analysis of caspase-7 in western blots

Lmyphoblastoid cells were treated in triplicate with 10 μg/ml bleomycin for 0h, 12h, 24h, and 48h. Caspase fragments were separated by SDS gel electrophoresis, using the primary antibody *cleaved Caspase-7* (Asp 198) and the second antibody (Anti-Mouse IgG Horsradish Peroxidase).

Detection of ATM and phosphorylated ATM (p-ATM) by immunoprecipitation

For examination of phosphorylation of ATM after bleomycin treatment, lymyphoblastoid cells in logarithmic growth were treated in triplicate with 0, 10, and 30 μg/ml bleomycin for 1 h at 37°C. Immunoprecipitation was performed with the FISH-antibody (Anti-ATM, rabbit polyclonal, Novus) and magnetic beads (Dynal Biotech ASA/Invitrogen). The separated proteins were probed with anti-ATM pS1981 (Rockland, monoclonal, mouse), and reprobed with an anti-ATM antibody (Abcam Cambrige, UK) [74].

Statistical analysis

The original data were exported to Excel 2007, GraphPad Prism 5 software, and SPSS 15.0 software for graphs and boxplots. The statistical tests used were Mann-Whitney U test, Fisher's exact test, and the unpaired t-test.

Analysis of chromosome fragility

Chromosome preparations were performed using standard techniques. The lymphoblastoid cell lines were analysed for chromosomal aberrations 4 h after irradiation (Muller MG 150 *x* ray apparatus; U_A, 100 kV; I, 10 mA; filter, 0.3 mm Ni; dose rate, 2.1 Gy/min;

Seifert, Hamburg, Germany) with 0 Gy, 0.5 Gy and 1.0 Gy including 1h colcemid treatment. 50 cells were analysed each. The types of aberrations were classified as achromatic lesions, chromatid and isochromatid breaks, and chromatid translocations. In order to calculate the total number of chromatid breaks per cell the latter were counted twice, the achromatic lesions and the telomere fusions neglected. Detailed protocols of the cytogenetic and molecular genetic methods are presented in [74].

Ethics statement

All procedures were performed in accordance with the ethical standards of the responsible committee. The cell lines were established with the ethical approval of "The Children's Memorial Health Institute, Warsaw", the Ethics Committee of the Second Medical School of Charles University in Prague, and the consent of the subjects, or their parents (for children and the fetus). The mouse studies were approved by the State Office for Health and Social, Berlin (G0438/09).

Data availability statement

The data that supports the findings of this study are available in the supplementary material of this article.

AUTHOR CONTRIBUTIONS

RH analyzed the telomere lengths in the framework of her dissertation (Q-PCR, Q-FISH, hTERT analysis). RK performed the caspase and ATM experiments in the framework of his dissertation. KC and ES took care of the subjects and performed the primary molecular diagnostics. RF provided fetal data and tissues. KJ and MW performed the TPE-OLD analysis and hTERT immortalization. ID performed the TRF analysis. RV performed and analysed array experiments. HN established and characterized the lymphoblastoid cell lines. MD provided resources. KS and MW drafted the paper. All authors read and accepted the manuscript.

ACKNOWLEDGMENTS

We acknowledge the probands and their parents for their participation, Annelore Junge for prenatal cytogenetic diagnostics, and André Nussenzweig for providing the humanized NBS mouse. We thank Antje Gerlach, Mohsen Karbasiyan, Janina Radszewski, and Bastian Salewsky for general technical assistance, Britta Teubner and Brigitte Schröder for cytogenetic assistance, and Dr. Rami Derbas for statistical advice. We would also like to thank Michael Hanna, PhD, (Mercury Medical Research & Writing) for proof-reading the manuscript.

CONFLICTS OF INTEREST

The authors declare that they have no conflicts of interest.

FUNDING

Raneem Habib received a stipend from the University of Damascus, Syria. Ryong Kim received a stipend from the Gottlieb Daimler- und Karl Benz-Stiftung. This work was supported by grants from the German Research Society to K.S. and M.D. (Collaborative Research Center 577, Project B1).

REFERENCES

1. Weemaes CM, Hustinx TW, Scheres JM, van Munster PJ, Bakkeren JA, Taalman RD. A new chromosomal instability disorder: the nijmegen breakage syndrome. Acta Paediatr Scand. 1981; 70:557–64. https://doi.org/10.1111/j.1651-2227.1981.tb05740.x PMID:7315300

2. Varon R, Demuth I, Chrzanowska KH. GeneReviews®: Nijmegen Breakage Syndrome. Seattle (WA); 1993. PMID:20301355

3. Demuth I, Digweed M. The clinical manifestation of a defective response to DNA double-strand breaks as exemplified by nijmegen breakage syndrome. Oncogene. 2007; 26:7792–98. https://doi.org/10.1038/sj.onc.1210876 PMID:18066092

4. Chrzanowska KH, Gregorek H, Dembowska-Bagińska B, Kalina MA, Digweed M. Nijmegen breakage syndrome (NBS). Orphanet J Rare Dis. 2012; 7:13. https://doi.org/10.1186/1750-1172-7-13 PMID:22373003

5. Saar K, Chrzanowska KH, Stumm M, Jung M, Nürnberg G, Wienker TF, Seemanová E, Wegner RD, Reis A, Sperling K. The gene for the ataxia-telangiectasia variant, nijmegen breakage syndrome, maps to a 1-cM interval on chromosome 8q21. Am J Hum Genet. 1997; 60:605–10. PMID:9042920

6. Varon R, Vissinga C, Platzer M, Cerosaletti KM, Chrzanowska KH, Saar K, Beckmann G, Seemanová E, Cooper PR, Nowak NJ, Stumm M, Weemaes CM, Gatti RA, et al. Nibrin, a novel DNA double-strand break repair protein, is mutated in nijmegen breakage syndrome. Cell. 1998; 93:467–76. https://doi.org/10.1016/s0092-8674(00)81174-5 PMID:9590180

7. Seemanova E, Varon R, Vejvalka J, Jarolim P, Seeman P, Chrzanowska KH, Digweed M, Resnick I, Kremensky I,

Saar K, Hoffmann K, Dutrannoy V, Karbasiyan M, et al. The slavic NBN founder mutation: a role for reproductive fitness? PLoS One. 2016; 11:e0167984. https://doi.org/10.1371/journal.pone.0167984 PMID:27936167

8. Seemanová E, Jarolim P, Seeman P, Varon R, Digweed M, Swift M, Sperling K. Cancer risk of heterozygotes with the NBN founder mutation. J Natl Cancer Inst. 2007; 99:1875–80. https://doi.org/10.1093/jnci/djm251 PMID:18073374

9. Digweed M, Sperling K. Nijmegen breakage syndrome: clinical manifestation of defective response to DNA double-strand breaks. DNA Repair (Amst). 2004; 3:1207–17. https://doi.org/10.1016/j.dnarep.2004.03.004 PMID:15279809

10. Rai R, Hu C, Broton C, Chen Y, Lei M, Chang S. NBS1 phosphorylation status dictates repair choice of dysfunctional telomeres. Mol Cell. 2017; 65:801–17.e4. https://doi.org/10.1016/j.molcel.2017.01.016 PMID:28216226

11. Oh J, Symington LS. Role of the Mre11 complex in preserving genome integrity. Genes (Basel). 2018; 9:589. https://doi.org/10.3390/genes9120589 PMID:30501098

12. Feldser D, Strong MA, Greider CW. Ataxia telangiectasia mutated (atm) is not required for telomerase-mediated elongation of short telomeres. Proc Natl Acad Sci USA. 2006; 103:2249–51. https://doi.org/10.1073/pnas.0511143103 PMID:16467146

13. Stracker TH, Petrini JH. The MRE11 complex: starting from the ends. Nat Rev Mol Cell Biol. 2011; 12:90–103. https://doi.org/10.1038/nrm3047 PMID:21252998

14. Cesare AJ, Reddel RR. Alternative lengthening of telomeres: models, mechanisms and implications. Nat Rev Genet. 2010; 11:319–30. https://doi.org/10.1038/nrg2763 PMID:20351727

15. Takai H, Smogorzewska A, de Lange T. DNA damage foci at dysfunctional telomeres. Curr Biol. 2003; 13:1549–56. https://doi.org/10.1016/s0960-9822(03)00542-6 PMID:12956959

16. Attwooll CL, Akpinar M, Petrini JH. The mre11 complex and the response to dysfunctional telomeres. Mol Cell Biol. 2009; 29:5540–51. https://doi.org/10.1128/MCB.00479-09 PMID:19667076

17. Dimitrova N, de Lange T. Cell cycle-dependent role of MRN at dysfunctional telomeres: ATM signaling-dependent induction of nonhomologous end joining (NHEJ) in G1 and resection-mediated inhibition of NHEJ in G2. Mol Cell Biol. 2009; 29:5552–63. https://doi.org/10.1128/MCB.00476-09 PMID:19667071

18. Verdun RE, Crabbe L, Haggblom C, Karlseder J. Functional human telomeres are recognized as DNA damage in G2 of the cell cycle. Mol Cell. 2005; 20:551–61. https://doi.org/10.1016/j.molcel.2005.09.024 PMID:16307919

19. Wu J, Zhang X, Zhang L, Wu CY, Rezaeian AH, Chan CH, Li JM, Wang J, Gao Y, Han F, Jeong YS, Yuan X, Khanna KK, et al. Skp2 E3 ligase integrates ATM activation and homologous recombination repair by ubiquitinating NBS1. Mol Cell. 2012; 46:351–61. https://doi.org/10.1016/j.molcel.2012.02.018 PMID:22464731

20. Kim JH, Grosbart M, Anand R, Wyman C, Cejka P, Petrini JH. The Mre11-Nbs1 interface is essential for viability and tumor suppression. Cell Rep. 2017; 18:496–507. https://doi.org/10.1016/j.celrep.2016.12.035 PMID:28076792

21. Holohan B, Wright WE, Shay JW. Cell biology of disease: telomeropathies: an emerging spectrum disorder. J Cell Biol. 2014; 205:289–99. https://doi.org/10.1083/jcb.201401012 PMID:24821837

22. Opresko PL, Shay JW. Telomere-associated aging disorders. Ageing Res Rev. 2017; 33:52–66. https://doi.org/10.1016/j.arr.2016.05.009 PMID:27215853

23. Siwicki JK, Degerman S, Chrzanowska KH, Roos G. Telomere maintenance and cell cycle regulation in spontaneously immortalized t-cell lines from nijmegen breakage syndrome patients. Exp Cell Res. 2003; 287:178–89. https://doi.org/10.1016/s0014-4827(03)00140-x PMID:12799193

24. Berardinelli F, Sgura A, Di Masi A, Leone S, Cirrone GA, Romano F, Tanzarella C, Antoccia A. Radiation-induced telomere length variations in normal and in nijmegen breakage syndrome cells. Int J Radiat Biol. 2014; 90:45–52. https://doi.org/10.3109/09553002.2014.859400 PMID:24168161

25. Habib R, Neitzel H, Ernst A, Wong JK, Goryluk-Kozakiewicz B, Gerlach A, Demuth I, Sperling K, Chrzanowska K. Evidence for a pre-malignant cell line

in a skin biopsy from a patient with nijmegen breakage syndrome. Mol Cytogenet. 2018; 11:17. https://doi.org/10.1186/s13039-018-0364-6 PMID:29445421

26. Lansdorp PM, Verwoerd NP, van de Rijke FM, Dragowska V, Little MT, Dirks RW, Raap AK, Tanke HJ. Heterogeneity in telomere length of human chromosomes. Hum Mol Genet. 1996; 5:685–91. https://doi.org/10.1093/hmg/5.5.685 PMID:8733138

27. Youngren K, Jeanclos E, Aviv H, Kimura M, Stock J, Hanna M, Skurnick J, Bardeguez A, Aviv A. Synchrony in telomere length of the human fetus. Hum Genet. 1998; 102:640–43. https://doi.org/10.1007/s004390050755 PMID:9703424

28. Habib R. Analysis of telomere length in patients with chromosomal instability syndromes, particularly Nijmegen Breakage Syndrome (NBS) and its mouse model by complementary technologies; Doctoral thesis Charité - Universitätsmedizin, 2012.

29. Difilippantonio S, Celeste A, Fernandez-Capetillo O, Chen HT, Reina San Martin B, Van Laethem F, Yang YP, Petukhova GV, Eckhaus M, Feigenbaum L, Manova K, Kruhlak M, Camerini-Otero RD, et al. Role of Nbs1 in the activation of the atm kinase revealed in humanized mouse models. Nat Cell Biol. 2005; 7:675–85. https://doi.org/10.1038/ncb1270 PMID:15965469

30. Sakellariou D, Chiourea M, Raftopoulou C, Gagos S. Alternative lengthening of telomeres: recurrent cytogenetic aberrations and chromosome stability under extreme telomere dysfunction. Neoplasia. 2013; 15:1301–13. https://doi.org/10.1593/neo.131574 PMID:24339742

31. Robin JD, Ludlow AT, Batten K, Magdinier F, Stadler G, Wagner KR, Shay JW, Wright WE. Telomere position effect: regulation of gene expression with progressive telomere shortening over long distances. Genes Dev. 2014; 28:2464–76. https://doi.org/10.1101/gad.251041.114 PMID:25403178

32. Zavadzkas JA, Plyler RA, Bouges S, Koval CN, Rivers WT, Beck CU, Chang EI, Stroud RE, Mukherjee R, Spinale FG. Cardiac-restricted overexpression of extracellular matrix metalloproteinase inducer causes myocardial remodeling and dysfunction in aging mice. Am J Physiol Heart Circ Physiol. 2008; 295:H1394–402. https://doi.org/10.1152/ajpheart.00346.2008 PMID:18689500

33. Schneider JE, Stork LA, Bell JT, ten Hove M, Isbrandt D, Clarke K, Watkins H, Lygate CA, Neubauer S. Cardiac structure and function during ageing in energetically compromised guanidinoacetate n-methyltransferase (GAMT)-knockout mice - a one year longitudinal MRI study. J Cardiovasc Magn Reson. 2008; 10:9. https://doi.org/10.1186/1532-429X-10-9 PMID:18275592

34. Herranz N, Gil J. Mechanisms and functions of cellular senescence. J Clin Invest. 2018; 128:1238–46. https://doi.org/10.1172/JCI95148 PMID:29608137

35. Kim KM, Noh JH, Bodogai M, Martindale JL, Pandey PR, Yang X, Biragyn A, Abdelmohsen K, Gorospe M. SCAMP4 enhances the senescent cell secretome. Genes Dev. 2018; 32:909–14. https://doi.org/10.1101/gad.313270.118 PMID:29967290

36. Anholt RR. Olfactomedin proteins: central players in development and disease. Front Cell Dev Biol. 2014; 2:6. https://doi.org/10.3389/fcell.2014.00006 PMID:25364714

37. Zhang X, Zhao G, Zhang Y, Wang J, Wang Y, Cheng L, Sun M, Rui Y. Activation of JNK signaling in osteoblasts is inversely correlated with collagen synthesis in age-related osteoporosis. Biochem Biophys Res Commun. 2018; 504:771–76. https://doi.org/10.1016/j.bbrc.2018.08.094 PMID:30217450

38. Marinelli S, Eleuteri C, Vacca V, Strimpakos G, Mattei E, Severini C, Pavone F, Luvisetto S. Effects of age-related loss of p/q-type calcium channels in a mice model of peripheral nerve injury. Neurobiol Aging. 2015; 36:352–64. https://doi.org/10.1016/j.neurobiolaging.2014.07.025 PMID:25150573

39. Cui H, Kong Y, Xu M, Zhang H. Notch3 functions as a tumor suppressor by controlling cellular senescence. Cancer Res. 2013; 73:3451–59. https://doi.org/10.1158/0008-5472.CAN-12-3902 PMID:23610446

40. Yang J, Liu K, Yang J, Jin B, Chen H, Zhan X, Li Z, Wang L, Shen X, Li M, Yu W, Mao Z. PIM1 induces cellular senescence through phosphorylation of UHRF1 at Ser311. Oncogene. 2017; 36:4828–42. https://doi.org/10.1038/onc.2017.96 PMID:28394343

41. Hua S, Ji Z, Quan Y, Zhan M, Wang H, Li W, Li Y, He X, Lu L. Identification of hub genes in hepatocellular carcinoma using integrated bioinformatic analysis. Aging (Albany NY). 2020; 12:5439–68. https://doi.org/10.18632/aging.102969 PMID:32213663

42. Park S, Park HEH, Son HG, Lee SJV. The role of RNA helicases in aging and lifespan regulation. Translational Medicine of Aging. 2017; 1:24–31. https://doi.org/10.1016/j.tma.2017.08.001

43. Zhao S, Weng YC, Yuan SS, Lin YT, Hsu HC, Lin SC, Gerbino E, Song MH, Zdzienicka MZ, Gatti RA, Shay JW, Ziv Y, Shiloh Y, Lee EY. Functional link between ataxia-telangiectasia and nijmegen breakage syndrome gene products. Nature. 2000; 405:473–77. https://doi.org/10.1038/35013083 PMID:10839544

44. Khincha PP, Dagnall CL, Hicks B, Jones K, Aviv A, Kimura M, Katki H, Aubert G, Giri N, Alter BP, Savage SA, Gadalla SM. Correlation of leukocyte telomere length measurement methods in patients with dyskeratosis congenita and in their unaffected relatives. Int J Mol Sci. 2017; 18:1765. https://doi.org/10.3390/ijms18081765 PMID:28805708

45. Meyer A, Salewsky B, Spira D, Steinhagen-Thiessen E, Norman K, Demuth I. Leukocyte telomere length is related to appendicular lean mass: cross-sectional data from the berlin aging study II (BASE-II). Am J Clin Nutr. 2016; 103:178–83. https://doi.org/10.3945/ajcn.115.116806 PMID:26675777

46. Kim W, Ludlow AT, Min J, Robin JD, Stadler G, Mender I, Lai TP, Zhang N, Wright WE, Shay JW. Regulation of the human telomerase gene TERT by telomere position effect-over long distances (TPE-OLD): implications for aging and cancer. PLoS Biol. 2016; 14:e2000016. https://doi.org/10.1371/journal.pbio.2000016 PMID:27977688

47. Compton SA, Choi JH, Cesare AJ, Ozgür S, Griffith JD. Xrcc3 and Nbs1 are required for the production of extrachromosomal telomeric circles in human alternative lengthening of telomere cells. Cancer Res. 2007; 67:1513–19. https://doi.org/10.1158/0008-5472.CAN-06-3672 PMID:17308089

48. Wu G, Jiang X, Lee WH, Chen PL. Assembly of functional ALT-associated promyelocytic leukemia bodies requires nijmegen breakage syndrome 1. Cancer Res. 2003; 63:2589–95. PMID:12750284

49. Barthel FP, Wei W, Tang M, Martinez-Ledesma E, Hu X, Amin SB, Akdemir KC, Seth S, Song X, Wang Q, Lichtenberg T, Hu J, Zhang J, et al. Systematic analysis of telomere length and somatic alterations in 31 cancer types. Nat Genet. 2017; 49:349–57. https://doi.org/10.1038/ng.3781 PMID:28135248

50. Krenzlin H, Demuth I, Salewsky B, Wessendorf P, Weidele K, Bürkle A, Digweed M. DNA damage in nijmegen breakage syndrome cells leads to PARP hyperactivation and increased oxidative stress. PLoS Genet. 2012; 8:e1002557. https://doi.org/10.1371/journal.pgen.1002557 PMID:22396666

51. Melchers A, Stöckl L, Radszewski J, Anders M, Krenzlin H, Kalischke C, Scholz R, Jordan A, Nebrich G, Klose J, Sperling K, Digweed M, Demuth I. A systematic proteomic study of irradiated DNA repair deficient Nbn-mice. PLoS One. 2009; 4:e5423. https://doi.org/10.1371/journal.pone.0005423 PMID:19412544

52. Petersen S, Saretzki G, von Zglinicki T. Preferential accumulation of single-stranded regions in telomeres of human fibroblasts. Exp Cell Res. 1998; 239:152–60. https://doi.org/10.1006/excr.1997.3893 PMID:9511733

53. Prowse KR, Greider CW. Developmental and tissue-specific regulation of mouse telomerase and telomere length. Proc Natl Acad Sci USA. 1995; 92:4818–22. https://doi.org/10.1073/pnas.92.11.4818 PMID:7761406

54. Blasco MA, Lee HW, Hande MP, Samper E, Lansdorp PM, DePinho RA, Greider CW. Telomere shortening and tumor formation by mouse cells lacking telomerase RNA. Cell. 1997; 91:25–34. https://doi.org/10.1016/s0092-8674(01)80006-4 PMID:9335332

55. Widmann TA, Herrmann M, Taha N, König J, Pfreundschuh M. Short telomeres in aggressive non-hodgkin's lymphoma as a risk factor in lymphomagenesis. Exp Hematol. 2007; 35:939–46. https://doi.org/10.1016/j.exphem.2007.03.009 PMID:17533048

56. Chrzanowska KH, Digweed M, Sperling K, Seemanova E, editors. DNA-repair deficiency and cancer: Lessons from lymphoma. Fulda: Wiley-VCH Verlag GmbH & Co. KGaA 2009.

57. Wentzensen IM, Mirabello L, Pfeiffer RM, Savage SA. The association of telomere length and cancer: a meta-analysis. Cancer Epidemiol Biomarkers Prev. 2011; 20:1238–50. https://doi.org/10.1158/1055-9965.EPI-11-0005 PMID:21467229

58. Jäger K, Walter M. Therapeutic targeting of telomerase. Genes (Basel). 2016; 7:39. https://doi.org/10.3390/genes7070039 PMID:27455328

59. Hahn WC. Role of telomeres and telomerase in the pathogenesis of human cancer. J Clin Oncol. 2003; 21:2034–43.

https://doi.org/10.1200/JCO.2003.06.018
PMID:12743159

60. Luo X, Sturgis EM, Yang Z, Sun Y, Wei P, Liu Z, Wei Q, Li G. Lymphocyte telomere length predicts clinical outcomes of HPV-positive oropharyngeal cancer patients after definitive radiotherapy. Carcinogenesis. 2019; 40:735–41. https://doi.org/10.1093/carcin/bgz019 PMID:30721961

61. Kolquist KA, Ellisen LW, Counter CM, Meyerson M, Tan LK, Weinberg RA, Haber DA, Gerald WL. Expression of TERT in early premalignant lesions and a subset of cells in normal tissues. Nat Genet. 1998; 19:182–86. https://doi.org/10.1038/554 PMID:9620778

62. Wolska-Kuśnierz B, Gregorek H, Chrzanowska K, Piątosa B, Pietrucha B, Heropolitańska-Pliszka E, Pac M, Klaudel-Dreszler M, Kostyuchenko L, Pasic S, Marodi L, Belohradsky BH, Čižnár P, et al, and Inborn Errors Working Party of the Society for European Blood and Marrow Transplantation and the European Society for Immune Deficiencies. Nijmegen breakage syndrome: clinical and immunological features, long-term outcome and treatment options - a retrospective analysis. J Clin Immunol. 2015; 35:538–49. https://doi.org/10.1007/s10875-015-0186-9 PMID:26271390

63. Li Y, Zhou G, Bruno IG, Zhang N, Sho S, Tedone E, Lai TP, Cooke JP, Shay JW. Transient introduction of human telomerase mRNA improves hallmarks of progeria cells. Aging Cell. 2019; 18:e12979. https://doi.org/10.1111/acel.12979 PMID:31152494

64. Aguado J, Sola-Carvajal A, Cancila V, Revêchon G, Ong PF, Jones-Weinert CW, Wallén Arzt E, Lattanzi G, Dreesen O, Tripodo C, Rossiello F, Eriksson M, d'Adda di Fagagna F. Inhibition of DNA damage response at telomeres improves the detrimental phenotypes of hutchinson-gilford progeria syndrome. Nat Commun. 2019; 10:4990. https://doi.org/10.1038/s41467-019-13018-3 PMID:31740672

65. Robin JD, Ludlow AT, Batten K, Gaillard MC, Stadler G, Magdinier F, Wright WE, Shay JW. SORBS2 transcription is activated by telomere position effect-over long distance upon telomere shortening in muscle cells from patients with facioscapulohumeral dystrophy. Genome Res. 2015; 25:1781–90. https://doi.org/10.1101/gr.190660.115 PMID:26359233

66. Martin GM. Genetic syndromes in man with potential relevance to the pathobiology of aging. Birth Defects Orig Artic Ser. 1978; 14:5–39. PMID:147113

67. Martin GM. Genetic modulation of senescent phenotypes in homo sapiens. Cell. 2005; 120:523–32. https://doi.org/10.1016/j.cell.2005.01.031 PMID:15734684

68. Hofer AC, Tran RT, Aziz OZ, Wright W, Novelli G, Shay J, Lewis M. Shared phenotypes among segmental progeroid syndromes suggest underlying pathways of aging. J Gerontol A Biol Sci Med Sci. 2005; 60:10–20. https://doi.org/10.1093/gerona/60.1.10 PMID:15741277

69. Neitzel H. A routine method for the establishment of permanent growing lymphoblastoid cell lines. Hum Genet. 1986; 73:320–26. https://doi.org/10.1007/BF00279094 PMID:3017841

70. Kannenberg F, Gorzelniak K, Jäger K, Fobker M, Rust S, Repa J, Roth M, Björkhem I, Walter M. Characterization of cholesterol homeostasis in telomerase-immortalized tangier disease fibroblasts reveals marked phenotype variability. J Biol Chem. 2013; 288:36936–47. https://doi.org/10.1074/jbc.M113.500256 PMID:24196952

71. Neuner B, Lenfers A, Kelsch R, Jäger K, Brüggmann N, van der Harst P, Walter M. Telomere length is not related to established cardiovascular risk factors but does correlate with red and white blood cell counts in a german blood donor population. PLoS One. 2015; 10:e0139308. https://doi.org/10.1371/journal.pone.0139308 PMID:26445269

72. Perner S, Brüderlein S, Hasel C, Waibel I, Holdenried A, Ciloglu N, Chopurian H, Nielsen KV, Plesch A, Högel J, Möller P. Quantifying telomere lengths of human individual chromosome arms by centromere-calibrated fluorescence in situ hybridization and digital imaging. Am J Pathol. 2003; 163:1751–56. https://doi.org/10.1016/S0002-9440(10)63534-1 PMID:14578175

73. Walter M, Forsyth NR, Wright WE, Shay JW, Roth MG. The establishment of telomerase-immortalized tangier disease cell lines indicates the existence of an apolipoprotein a-I-inducible but ABCA1-independent cholesterol efflux pathway. J Biol Chem. 2004; 279:20866–73. https://doi.org/10.1074/jbc.M401714200 PMID:15001567

74. Kim R. Assoziationsstudie zur klinischen Variabilität bei Patienten mit dem Nijmegen Breakage Syndrom; Doctoral thesis Charité - Universitätsmedizin, 2010.

SUPPLEMENTARY MATERIALS

Supplementary Figures

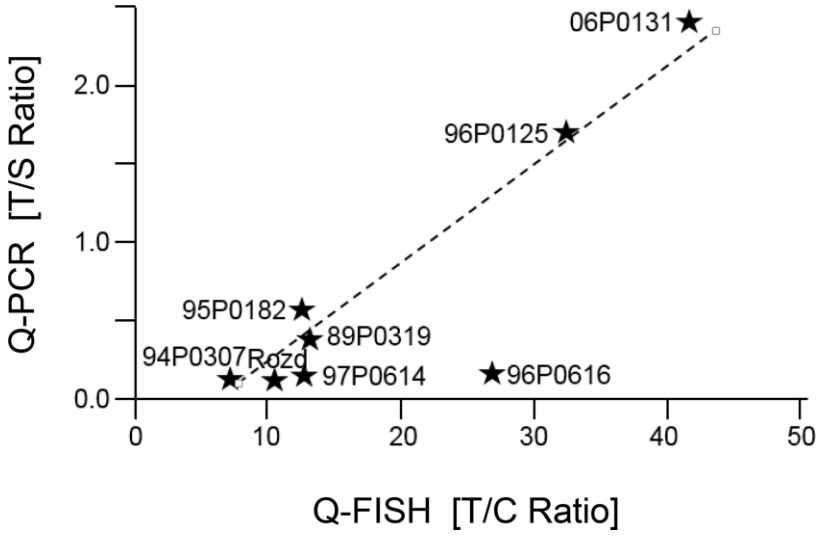

Supplementary Figure 1. Correlation between telomere length analyzed by qPCR and Q-FISH in six NBS lymphoblastoid cell lines and two controls (06P0131,96P0125). Original from [28].

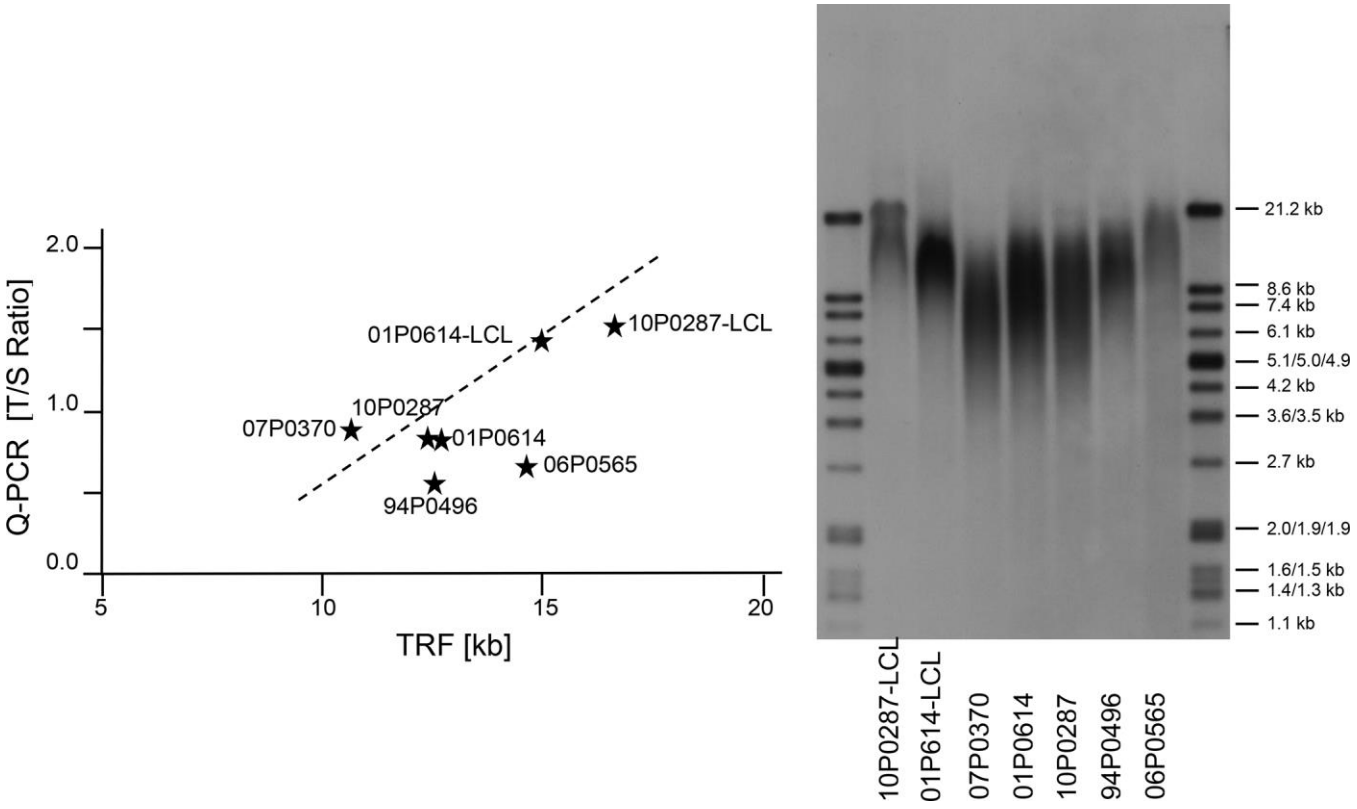

Supplementary Figure 2. Correlation of telomere length measured by qPCR and TRF analysis. The equation of the computed regression line is y= 3.4(X) +10.11 with a correlation coefficient of r= 0.64. Mean TRF length has been defined according to the formula described in Roche Application Note No. 12 209 136 001 (April 2018).

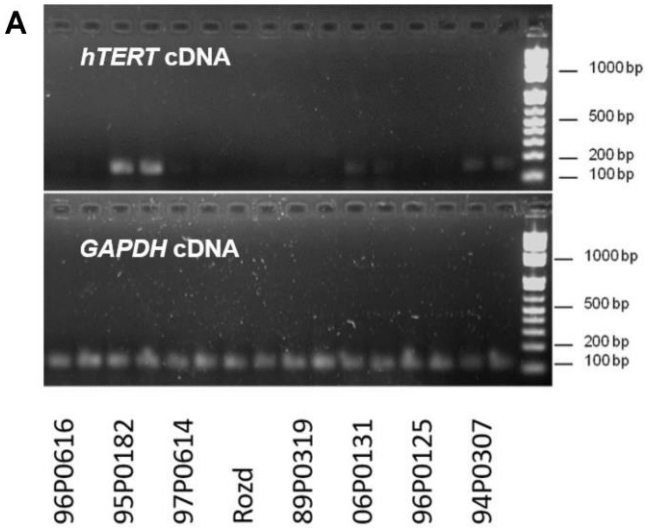
A
hTERT cDNA
1000 bp
500 bp
200 bp
100 bp
GAPDH cDNA
1000 bp
500 bp
200 bp
100 bp
96P0616
95P0182
97P0614
Rozd
89P0319
06P0131
96P0125
94P0307

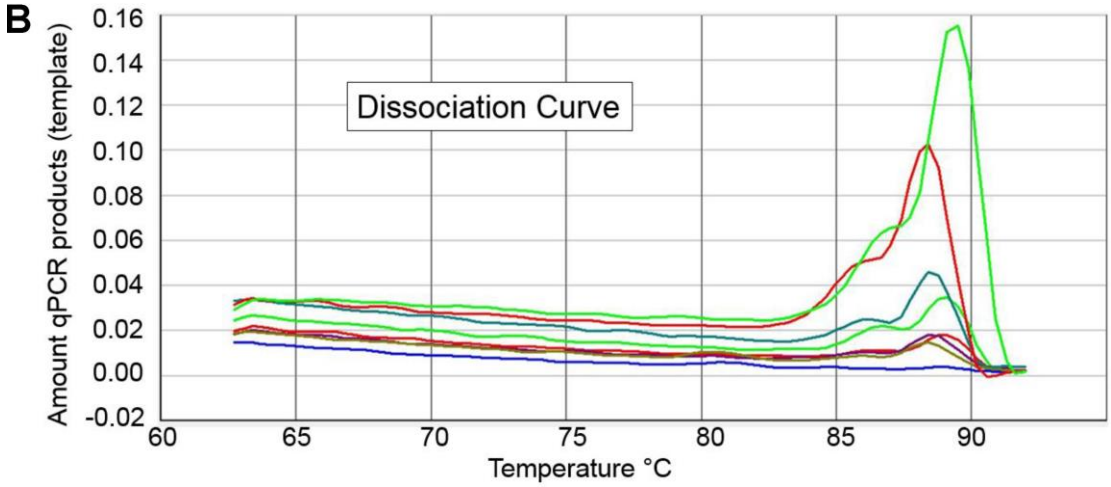
B
Dissociation Curve
Amount qPCR products (template)
0.16
0.14
0.12
0.10
0.08
0.06
0.04
0.02
0.00
-0.02
60
65
70
75
80
85
90
Temperature °C

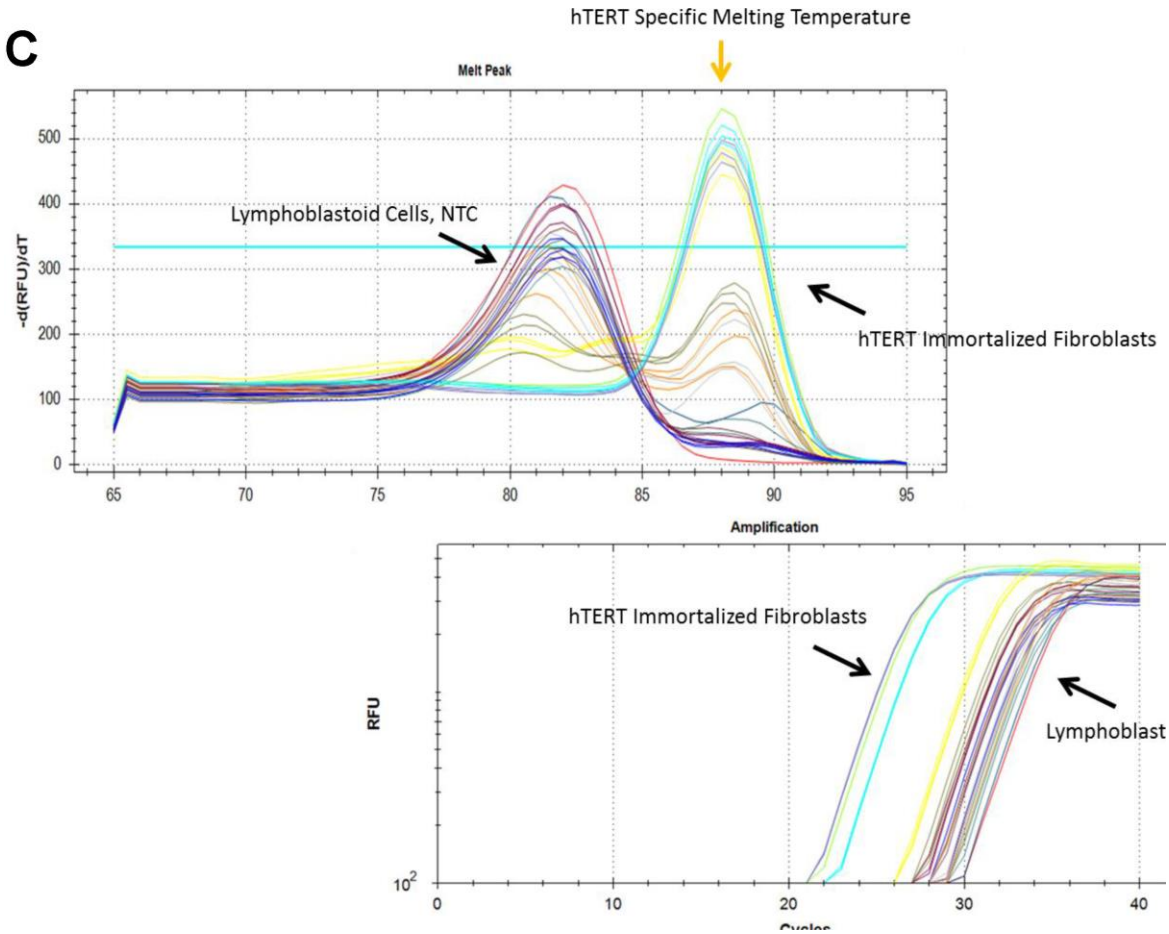

Supplementary Figure 3. (**A**) Expression of the *hTERT* gene in lymphoblastoid cell lines (LCLs) and *hTERT* immortalized fibroblasts. Agarose gel electrophoresis of the PCR products of the *hTERT* cDNA and the GAPDH cDNA as internal control. 06P0131 and 96P0125 are LCL controls derived from male individuals homozygous for the wild type allele. Original from [28]. (**B**) Expression of *hTERT* as measured by qPCR. Dissociation curve of qPCR for *hTERT* cDNA (template). The high fluorescent peaks correspond to 95P0182 (green) and 94P0307 (red). The weak fluorescent peaks correspond to 06P0131 (dark green) and 97P0614 (light green). The lower lines (no template) correspond to 89P0319 (purple), 96P0616 (red), Rozd (brown) and 96P0125 (blue). (**C**) Expression of *hTERT* as measured by qPCR in a separate experiment. Dissociation curve of qPCR for *hTERT* cDNA (template) and non template control (NTC).

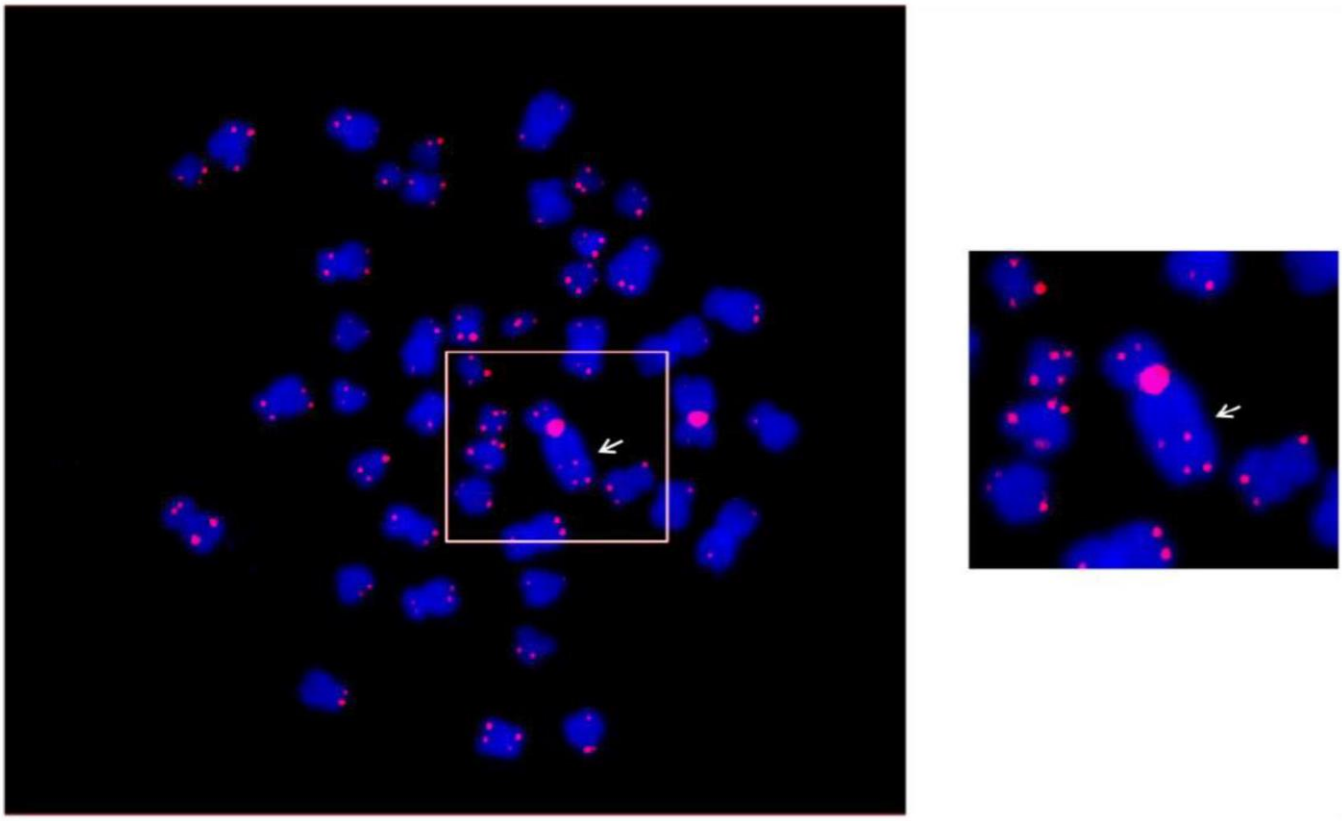

Supplementary Figure 4. Metaphase of NBS-LCL 94P0307 after Q-FISH. The arrow points to the telomere fusion between p telomere of chromosome 2 and an undefined chromosome.

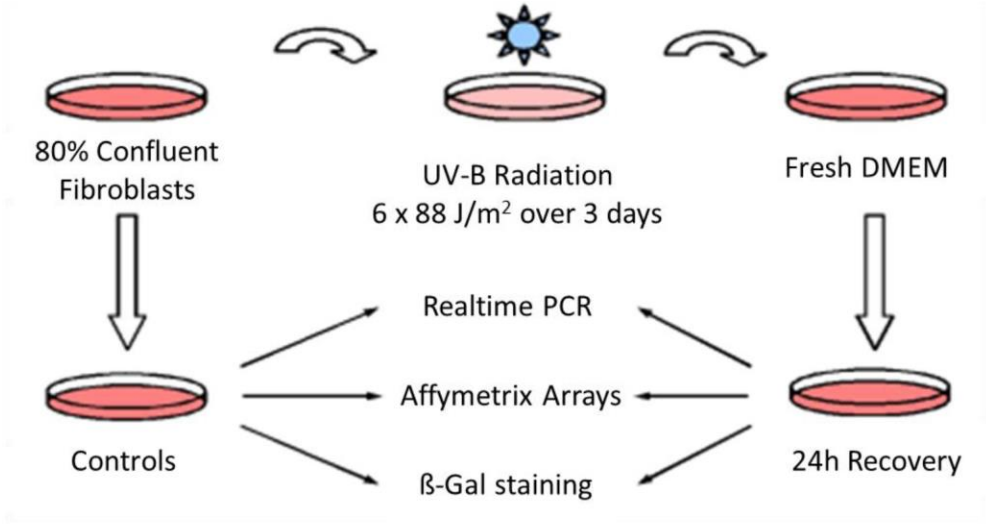

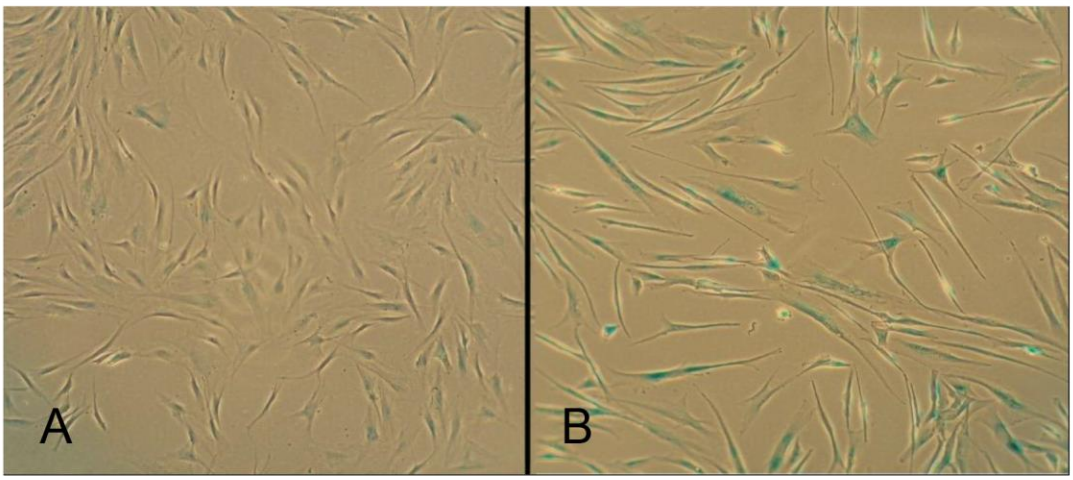

Supplementary Figure 5. TPE-OLD candidate gene approach - UV-Radiation. Human skin fibroblasts at 80 % confluence were exposed to UV-B radiation in a thin layer of DMEM using four 20W TL/12 lamps emitting broadband UV-B peaking at 312 nm. The procedure was performed twice a day for 3 consecutive days with a total dose of 528 J/m². 24 hours after the last irradiation analysis β galactosidase staining was performed. A, pre-treatment. B, senescent cells.

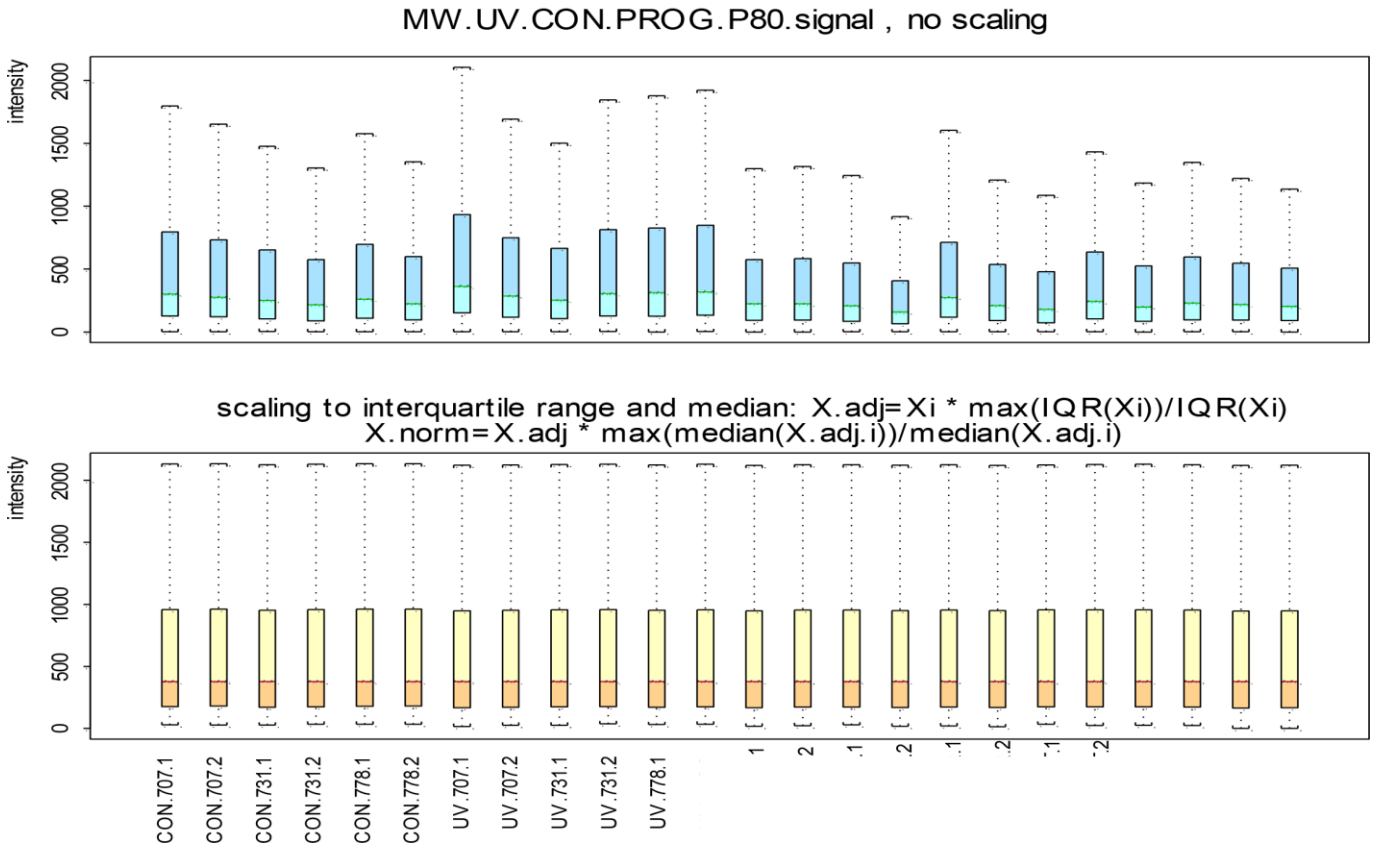

Supplementary Figure 6. TPE-OLD candidate gene approach – Statistical analysis. The unnormalized raw data of all experiments were exported in an ASCII format from the Affymetrix GCOS®-Software and imported in the statistical platform S-Plus 8.0® (Insightful Corporation, Seattle, Washington). Ten experiments were assigned two groups based on the characteristics of UV-treatment (6 repeats) and pre-senescence (4 repeats). Both groups were compared to six control experiments. The aim was to identify the most relevant genes discriminating between cells with UV-treatment and cells from pre-senescence, HGP). For this purpose a computer program based on S-Plus which computes the required subsets of genes and simultaneously controls the overall false positive rate was used. 16 microarrays were analyzed, each with 54.675 transcripts on an HGU133-A2.0 array from Affymetrix®, in a design with 3 groups, each with 4-6 replicates. To keep the data at a high quality level we used the GCOS Detection calls to discard all genes (transcripts) with callrates lower than 80% present in at least 13 of 16 repeats in a total of 19.984 transcripts. To make the data of different microarrays comparable, the Affymetrix-GCOS Signal-values were first normalized to have the same interquartile range (IQR) as the maximum IQR of the set and then each chip's median was shifted to the maximum median of the chip set.

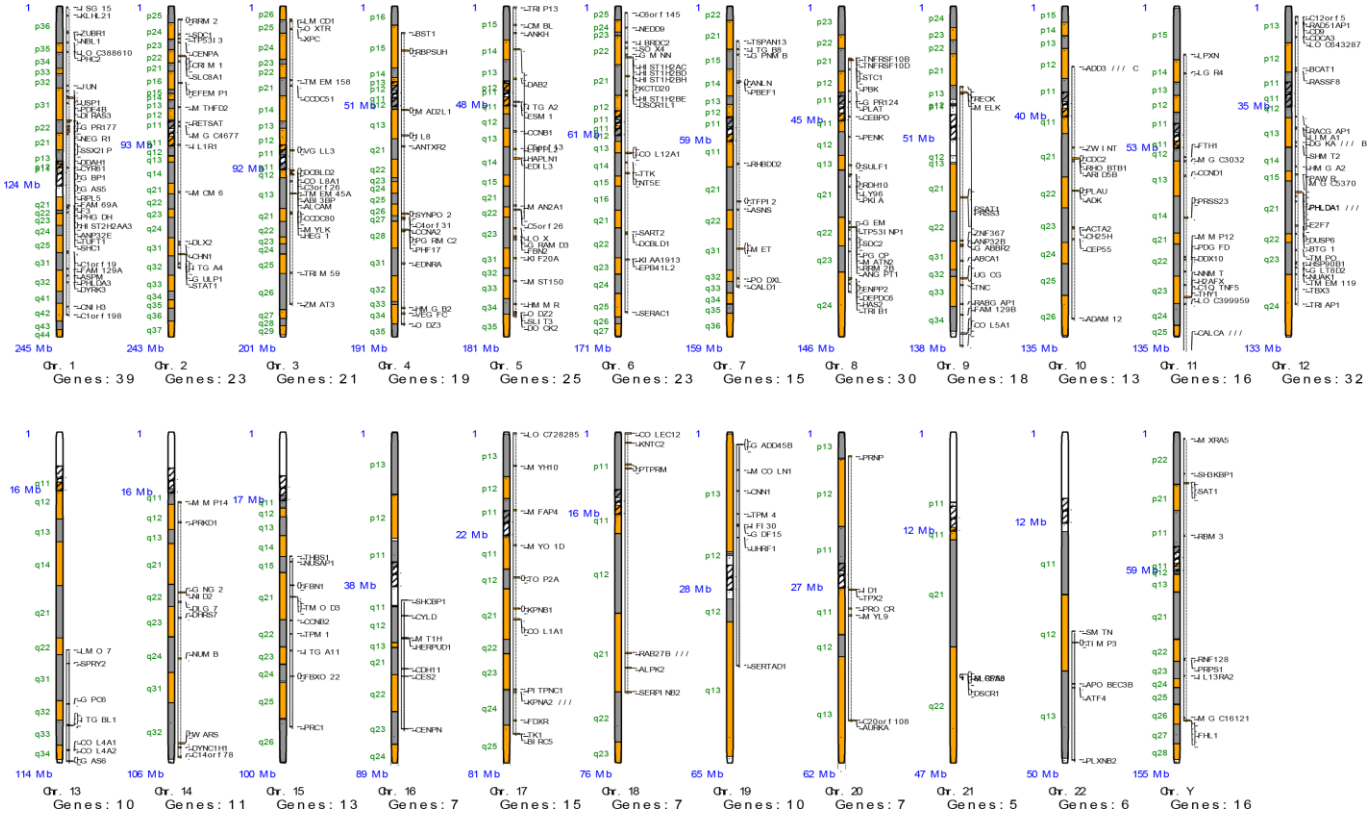

Supplementary Figure 7. TPE-OLD candidate gene approach. Differentially expressed genes (DEGs), dependent on chromosomal localization. For simplification only the DEGs with highest significance level are shown.

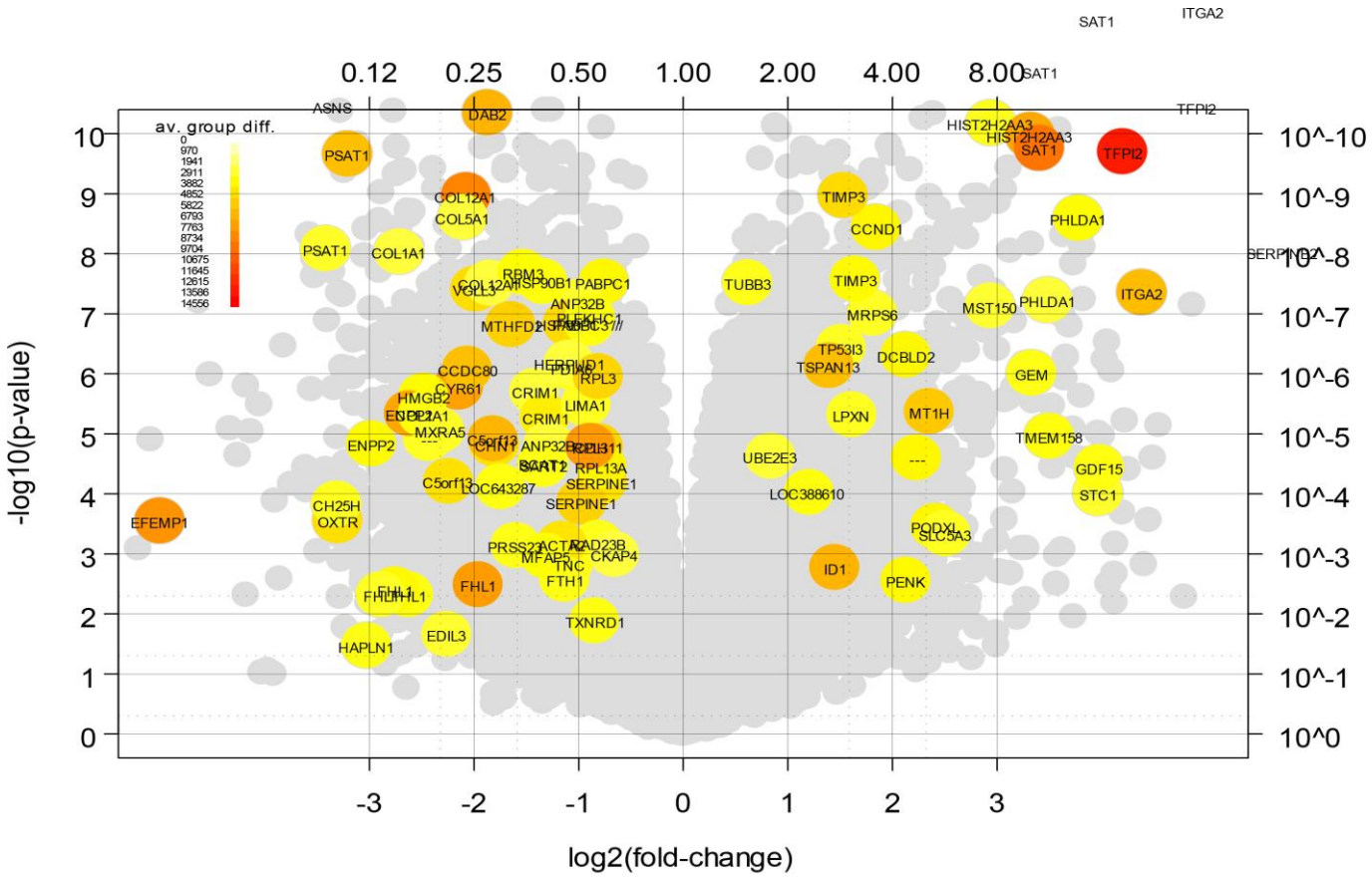

Figure 1 . Volcano plot from MW.UV.CON
Diff < -3000 , p<= 0.05 , fc < 0.67 , F-p <= 0.05 (n= 60) , diff >= 3000 , fc >= 1.5 (n= 34 entries)
Comparisons: 54675 , observed differences (pvalue <= 0.05): 15841 , false detection rate: 0.17

Supplementary Figure 8. TPE-OLD candidate gene approach. Differentially expressed genes (DEGs), visualized as Volcano Plot.

Supplementary Tables

Supplementary Table 1. Telomere length of healthy individuals (controls).

DNA number	relative telomere length	Age (years)	Sex
04P0523	2.16	1	F
04P0862	3.41	1	F
05P0586	1.6	2	M
05P0509	1.12	2	F
04P0535	1.45	3	F
01P0888	0.9	3	M
02P01053	2.25	5	M
04P0216	1.42	9	M
112	1.37	11	F
204	1.29	11	F
166	1.83	12	F
17	1.94	13	F
443	1.93	14	F
444	1.36	15	M
210	0.98	16	F
365	1.51	17	F
247	1.23	18	F
47	1.17	19	F
293	1.58	19	-
193	0.74	20	M
390	1.41	20	M
431	1.25	20	M
423	0.79	20	M
11	1.2	20	M
161	1	20	F
420	0.73	20	F
o2	1	21	M
440	1	21	F
143	1.26	21	F
448	0.83	21	F
129	0.93	21	F
169	1.16	21	F
164	1.18	21	F
13	1.22	21	M
413	0.9	21	F
223	1	22	F
163	0.95	22	M
40	0.91	22	F
188	0.76	22	F
241	1	23	M
246	0.84	23	M
470	1	23	M
280	1.44	23	F
262	0.99	23	F
191	0.89	23	F
328	0.78	24	M
333	1.14	24	F
471	1.39	24	F
464	0.75	24	M
284	1	24	F
150	1	24	F
330	0.85	24	F
292	1.26	24	M
o1	0.97	25	F

425	0.81	25	F
49	1.65	25	F
165	0.99	25	F
189	0.92	25	M
323	1.33	25	M
90	0.84	26	F
320	1.23	26	F
93	1.72	26	F
41	1.52	26	F
388	0.78	27	F
147	0.75	27	F
303	1.34	27	F
445	0.88	27	F
430	0.84	27	F
102	1.3	27	F
32	1	28	M
313	1.54	28	F
160	0.94	28	M
472	0.73	28	F
347	1	28	F
146	0.74	28	M
222	1.1	28	F
Ra	1	28	F
305	1.51	29	F
383	0.92	29	F
207	1	29	F
37	0.81	29	M
73	1.12	29	M
187	0.96	29	M
104	0.74	29	F
23	0.71	29	-
31	0.92	30	F
269	0.84	30	F
1	0.88	30	M
271	1.23	30	F
372	0.93	30	M
27	0.75	30	-
595	1.71	35	M
188	1.21	37	M
596	0.88	38	M
192	0.78	39	M
597	0.94	40	-
194	1	43	F
584	0.79	45	-
591	0.53	60	F
592	0.51	60	M
579	0.4	64	M
590	0.47	66	M
570	0.56	67	M
574	0.5	74	M
588	0.51	75	F
572	0.61	78	F
580	0.61	78	M
587	0.61	80	M

Age group	Number	Mean	SD	Max	Min
1-10	8	1.79	0.80	3.41	0.9
11-20	18	1.30	0.37	1.94	0.73
21-30	65	1.03	0.24	1.72	0.71
31-45	7	1.04	0.33	1.71	0.78
46-80	10	0.53	0.07	0.61	0.4

Supplementary Table 2. Estimation of telomere length of NBS-homozygotes.

DNA number	Relative telomere lengths	Age (years)	Sex
13720	1.62	1	M
12207	1.48	1	M
13424	1.29	1	F
6645	0.3	1	F
5342	0.21	1	M
6018	0.68	2	F
7105	0.44	2	F
3769	0.43	2	M
3772	0.43	2	F
7694	2.1	3	F
11766	2	3	F
8294	2.1	3	F
13607	0.98	5	F
13028	1.55	6	M
3426	1.35	6	F
8165	1	6	M
9990	1.3	6	M
11348	1.17	7	F
5202	0.67	7	F
3201	0.35	7	F
4530	0.22	7	F
8304	0.34	8	M
12557	1.13	8	-
5700	0.99	9	F
11154	1.73	10	M
7822	0.96	10	M
9028	0.78	10	F
5546	0.58	10	M
6023	1.3	12	F
13921	0.76	12	M
2552	0.69	13	M
3197	0.2	13	M
3205	1.3	14	M
3316	0.29	15	M
5567	0.64	15	M
5450	0.56	18	F
10376	0.46	19	F
5431	0.26	20	F

1-10 years:

Category	Number	Mean	SD	Max	Min
Control	8	1.79	0.80	3.41	0.90
NBS-Homozygote	28	1.01	0.58	2.10	0.21

11-20 years

Category	Number	Mean	SD	Max	Min
Control	18	1.30	0.37	1.94	0.73
NBS-Homozygote	10	0.65	0.39	1.30	0.20

Supplementary Table 3. Estimation of telomere length of NBS-heterozygotes.

DNA number	Relative telomere lengths	Age (years)	Sex
5343	2	1	F
10130	1.51	2	M
4328	0.89	3	M
8296	1.68	3	M
3221	1	4	M
3223	2	5	F
10133	1.38	5	F
10131	0.99	5	M
10123	2.35	7	M
7234	1.56	8	F
6017	1.77	8	M
3224	1.49	10	M
10120	0.71	12	F
4787	1.31	19	M
8295	0.71	22	F
3222	1	25	F
10124	2	25	M
508	1	27	F
6024	1.3	30	F
466	1.3	30	M
7235	0.79	30	M
7824	0.75	33	M
7823	0.78	35	M
6025	0.32	40	M
4786	0.25	40	M
464	0.6	50	F
463	0.27	54	M

Age	Category	Number	Mean	SD	Max	Min
1 -- 10	Control	8	1.79	0.80	3.41	0.90
	NBS-Heterozygote	12	1.55	0.45	2.35	0.89
11 -- 30	Control	83	1.08	0.29	1.94	0.71
	NBS-Heterozygote	9	1.12	0.41	2.00	0.71
	Control	17	0.74	0.33	1.71	0.40
	NBS-Heterozygote	6	0.50	0.24	0.78	0.25

Supplementary Table 4. Analysis of chromosome fragility after irradiation in six NBS lymphoblastoid cell lines with the absolute longest (above) and absolute shortest (below) telomere lengths.

	Survival (y)	Aberrant mitoses (%)			Breaks (%)		
		0 Gy	0,5 Gy	1,0 Gy	0 Gy	0,5 Gy	1,0 Gy
89P0319 ♀	0	14	69	88	0.16	1.42	2.2
96P0616 ♀	0,2	2	38	42	0.02	0.54	0.68
95P0182 ♀	2,8	0	42	100	0	1.18	3.5
Mean ± SD		**5 ± 8**	**50 ± 7**	**77 ± 31**	**0.16 ± 0,02**	**1.05 ± 0,45**	**2.13 ± 1,41**
97P0614 ♂	>12	2	40	42	0.04	0.52	0.66
RoZd ♀	>12	0	39	59	0	0.48	0.71
94P0307 ♂	>12	0	42	72	0	1.16	1.58
		1 ± 1	**40 ± 2**	**58 ± 15**	**0.01 ± 0.02**	**0.72 ± 0.38**	**0.98 ± 0.52**
Control		**0**	**16**	**10**	**0**	**0.2**	**0.14**

Chromatid breaks were distinguished from chromatid translocations. Since the latter are due to two breakage events, they were counted twice for the calculation of the total break events. Dicentric chromosomes were not scored because they cannot be induced in the G2 phase and apparently are due to telomere fusions.

Supplementary Table 5. T/C-FISH data on telomere lengths of NBS-LCL 94P0307.

Chromosome	Median (± SD) of p-arm	Median (± SD) of q-arm
1	8.7 (±4.8)	8 (±5.9)
2	5.2 (±4.5)	5.1(±8.3)
3	9.0 (±9.3)	9.9 (±6.1)
4	11.2(±10.1)	7.2(±10.5)
5	9.1(±5.7)	11.4(±11.1)
6	9.1(±7.1)	7.8(±4.8)
7	10.6(±6.1)	4.9(±6.7)
8	9.3 (±6.3)	7.1(±6.6)
9	10.7(±5.9)	7.3(±5.5)
10	10.2(±9.4)	17.4(±11.1)
11	9.5(±6.5)	7 (±5.6)
12	8.9(±5.2)	7.5(±5.4)
13	5.6(±6.1)	8.6(±7.3)
14	6.4(±7.3)	9.8(±6.9)
15	5.5(±4.5)	9.7(±4.9)
16	7.5(±6.5)	8.1(±5.1)
17	5 (±4.6)	6.1(±5.7)
18	6.9(±6.2)	5.8(±6.6)
19	13.2(±36.6)	6.2(±5.9)
20	5.3(±4.2)	6.7(±4.1)
21	4.6(±3.2)	6.2(±6.1)
22	5.7(±3.5)	4.9(±3.3)
X	6.6(±7.1)	6.1(±7.9)
Y	6.3(±3.3)	4.5(±5.1)

Supplementary Table 6. Q-FISH analysis of telomere lengths of the p arm of chromosome 19 in 11 metaphases of the NBS lymphoblastoid cell line 94P0307. T/C values are presented for the highly and weakly fluorescent chromosome 19.

Metaphase	1	2	3	4	5	6	7	8	9	10	11	∅
T/C value: high	85.2	52.6	47.1	44.1	60.5	33.4	79.4	60.2	32.9	68.3	58.6	56.6
T/C value: low	3.2	12.6	2.0	2.1	8.2	1.1	2.1	6.3	2.2	3.5	9.6	4.8

Supplementary Table 7A. TPE-OLD candidate gene approach using Affymetrix expression data in senescent (HGP), *hTERT* immortalized senescent and UV-B-treated fibroblasts for comparison. In yellow those genes with highly significant expression changes in senescent but not in UV-B-treated and/or not in *hTERT* immortalized senescent fibroblasts.

Gene Symbol (iReports)	Chromosome location	Gene description	c=changed, ---=known, u=unknown)	Gene Symbol (Affymetrix)	Probe Set ID	HGP vs. CON: Gene Symbol (Affymetrix)	P-Value	Entrez Gene ID	Fold Change	Probe Set ID	Source
BSG	571,297-583,493		---	BSG	208677_s_at	BSG	0,0000001809	682	2,840	208677_s_a	HGP
BTBD2	1,985,447-2,034,880		---	BTBD2	207722_s_at	BTBD2	0,0000003871	55643	2,024	207722_s_a	HGP
CACNA1A	13,317,256-13,734,804		---	CACNA1A	206399_x_at	CACNA1A	0,0001904053	773	2,096	206399_x_a	HGP
COL5A3	10,070,237-10,121,147		---	COL5A3	218975_at	COL5A3	0,0207965844	50509	2,367	218975_at	HGP
DDX39A	14,519,610-14,530,195	DEAD (Asp-	c	DDX39	201584_s_at	DDX39	0,0000313020	10212	-2,033	201584_s_a	HGP
FKBP8	18,531,751-18,544,077		---	FKBP8	208255_s_at	FKBP8	0,0000000564	23770	3,060	208255_s_a	HGP
FKBP8	18,531,751-18,544,077		---	FKBP8	40850_at	FKBP8	0,0000002468	23770	2,710	40850_at	HGP
GAMT	1,397,088-1,401,569		---	GAMT	205354_at	GAMT	0,0000137147	2593	2,071	205354_at	HGP
GAMT	1,397,088-1,401,569		---	GAMT	1552474_a_at	GAMT	0,0000009301	2593	2,006	1552474_a_	HGP
ICAM1	10,381,511-10,397,291		---	ICAM1	202638_s_at	ICAM1	0,0068949400	3383	3,355	202638_s_a	HGP
ICAM1	10,381,511-10,397,291		---	ICAM1	202637_s_at	ICAM1	0,0015622485	3383	2,182	202637_s_a	HGP
ISYNA1	18,545,198-18,549,111		---	ISYNA1	222240_s_at	ISYNA1	0,0004248998	51477	2,104	222240_s_a	HGP
JUND	18,390,563-18,392,432		---	JUND	203751_x_at	JUND	0,0000014634	3727	2,581	203751_x_a	HGP
JUND	18,390,563-18,392,432		---	JUND	214326_x_at	JUND	0,0000020790	3727	2,695	214326_x_a	HGP
MAP2K2	4,090,319-4,124,126		---	MAP2K2	213490_s_at	MAP2K2	0,0000007541	5605	2,068	213490_s_a	HGP
MARCH2	8,478,154-8,503,901		---	MARCH2	210075_at	MARCH2	0,0001449725	51257	2,193	210075_at	HGP
NOTCH3	15,159,038-15,200,981		---	NOTCH3	203238_s_at	NOTCH3	0,0112953135	4854	4,109	203238_s_a	HGP
OLFM2	137,967,268-138,013,025		---	OLFM2	223601_at	OLFM2	0,0066981369	93145	3,824	223601_at	HGP
PALM	708,953-748,330		---	PALM	203859_s_at	PALM	0,0023807474	5064	3,551	203859_s_a	HGP
RAB11B	8,454,865-8,469,318		---	RAB11B	34478_at	RAB11B	0,0000104773	9230	2,245	34478_at	HGP
RNASEH2A	12,917,394-12,924,462		---	RNASEH2A	203022_at	RNASEH2A	0,0005021651	10535	-2,063	203022_at	HGP
SCAMP4	1,905,213-1,926,016		---	SCAMP4	213244_at	SCAMP4	0,0000004595	113178	2,707	213244_at	HGP
SCAMP4	1,905,213-1,926,016		---	SCAMP4	235073_at	SCAMP4	0,0000035546	113178	2,345	235073_at	HGP
SLC44A2	10,713,121-10,755,235		---	SLC44A2	225175_s_at	SLC44A2	0,0005098295	57153	2,045	225175_s_a	HGP
SYDE1	15,218,214-15,225,799		---	SYDE1	216272_x_at	SYDE1	0,0027395466	85360	2,014	216272_x_a	HGP
SYDE1	15,218,214-15,225,799		---	SYDE1	212962_at	SYDE1	0,0012149194	85360	2,699	212962_at	HGP
SYDE1	15,218,214-15,225,799		---	SYDE1	216271_x_at	SYDE1	0,0005825874	85360	2,208	216271_x_a	HGP
UHRF1	4,903,092-4,962,165		---	UHRF1	225655_at	UHRF1	0,0000692885	29128	-2,653	225655_at	HGP
XAB2	7,684,411-7,694,451		---	XAB2	218110_at	XAB2	0,0000618183	56949	2,160	218110_at	HGP

iReports Results

Gene Symbol (iReports)	HGP-TERT vs. CON: Gene Symbol (Affymetrix)	P-Value	Entrez Gene ID	Fold Change	Probe Set ID	Source	UV vs. CON: Gene Symbol (Affymetrix)	P-Value	Entrez Gene ID	Fold Change	Probe Set ID	Source
BSG	BSG	0,0000076921	682	2,123	208677_s_a	HGP-TERT						
BTBD2	BTBD2	0,0000042508	55643	2,436	207722_s_a	HGP-TERT						
CACNA1A												
COL5A3												
DDX39A												
FKBP8	FKBP8	0,0000458219	23770	2,616	208255_s_a	HGP-TERT						
FKBP8	FKBP8	0,0000205907	23770	3,075	40850_at	HGP-TERT						
GAMT												
GAMT												
ICAM1	ICAM1	0,0045024336	3383	2,718	202638_s_a	HGP-TERT						
ICAM1												
ISYNA1							ISYNA1	0,0000632685	51477	3,151	222240_s_a	UV
JUND	JUND	0,0000122462	3727	2,480	203751_x_a	HGP-TERT						
JUND	JUND	0,0000132107	3727	2,780	214326_x_a	HGP-TERT						
MAP2K2	MAP2K2	0,0000168467	5605	2,866	213490_s_a	HGP-TERT						
MARCH2	MARCH2	0,0003620400	51257	2,099	210075_at	HGP-TERT						
NOTCH3												
OLFM2												
PALM	PALM	0,0034745851	5064	2,405	203859_s_a	HGP-TERT						
RAB11B	RAB11B	0,0020523284	9230	2,312	34478_at	HGP-TERT						
RNASEH2A												
SCAMP4	SCAMP4	0,0000100484	113178	2,738	213244_at	HGP-TERT						
SCAMP4												
SLC44A2	SLC44A2	0,0009311980	57153	2,094	225175_s_a	HGP-TERT						
SYDE1												
SYDE1	SYDE1	0,0104646032	85360	2,060	212962_at	HGP-TERT						
SYDE1												
UHRF1							UHRF1	0,0000024303	29128	-4,123	225655_at	UV
XAB2	XAB2	0,0000488575	56949	2,306	218110_at	HGP-TERT						

Supplementary Table 7B. TPE-OLD candidate gene approach using Affymetrix expression data in senescent cells, *hTERT* immortalized senescent cells and UV-B-treated cells, Raw data.

Raw data of Affymetrix experiments

Row	in HGP, HGP-TERT & UV?	SEN vs. CON: RowNames	Fold Change	SIG	Gene.Symbol	Physical.Position	UniGene.ID
9	0	208677_s_a	2,484	****	BSG	572564	Hs.501293
10	0	207722_s_a	2,213	****	BTBD2	1985446	Hs.465543
11	0	206399_x_a	1,432	**	CACNA1A	13318114	Hs.501632
14	0	218975_at	3,604	*	COL5A3	10070236	Hs.235368
15	0	201584_s_a	-1,806	***	DDX39	14519626	Hs.311609
16	0	208255_s_a	4,278	****	FKBP8	18642572	Hs.173464
17	0	40850_at	3,360	****	FKBP8	18642572	Hs.173464
18	0	205354_at	2,434	****	GAMT	1397087	Hs.81131
19	0	1552474_a_	2,191	****	GAMT	1398451	Hs.81131
20	0	202638_s_a	3,470	**	ICAM1	10381778	Hs.643447
21	0	202637_s_a	3,260	*	ICAM1	10381763	Hs.643447
22	0	222240_s_a	3,428	***	ISYNA1	18545631	Hs.724523
23	0	203751_x_a	3,096	****	JUND	18390570	Hs.2780
24	0	214326_x_a	2,945	****	JUND	18391013	Hs.2780
26	0	213490_s_a	1,820	****	MAP2K2	128766471	Hs.465627
27	0	210075_at	2,496	***	MARCH2	8486669	Hs.631861
30	0	203238_s_a	4,695	**	NOTCH3	15270444	Hs.8546
31	0	223601_at	9,557	*	OLFM2	9964399	Hs.169743
32	0	203859_s_a	2,897	**	PALM	709001	Hs.631841
37	0	34478_at	2,002	***	RAB11B	8454778	Hs.626404
38	0	203022_at	-2,272	**	RNASEH2A	12917438	Hs.532851
39	0	213244_at	2,225	****	SCAMP4	1925044	Hs.144980
40	0	235073_at	1,723	**	SCAMP4	1905405	Hs.144980
41	0	225175_s_a	1,863	**	SLC44A2	10754489	Hs.534560
42	0	216272_x_a	2,756	*	SYDE1	15223120	Hs.706845
43	0	212962_at	2,645	**	SYDE1	15220561	Hs.528701
44	0	216271_x_a	2,217	**	SYDE1	15218244	Hs.528701
47	0	225655_at	-2,371	**	UHRF1	20704503	Hs.108106
48	0	218110_at	2,304	****	XAB2	7684411	Hs.9822

Row	SEN-TERT vs. CON: RowNames	Fold Change	SIG	Gene.Symbol	pq	Chromosome	Physical.Position	UniGene.ID
9	208677_s_a	-1,203	**	BSG	19p13.3	19	572564	Hs.501293
10	207722_s_a	-1,030	n	BTBD2	19p13.3	19	1985446	Hs.465543
11	206399_x_a	1,082	n	CACNA1A	19p13.2-p1	19	13318114	Hs.501632
14	218975_at	-1,417	n	COL5A3	19p13.2	19	10070236	Hs.235368
15	201584_s_a	1,356	n	DDX39	19p13.12	19	14519626	Hs.311609
16	208255_s_a	1,004	n	FKBP8	19p12	19	18642572	Hs.173464
17	40850_at	1,088	n	FKBP8	19p12	19	18642572	Hs.173464
18	205354_at	1,423	*	GAMT	19p13.3	19	1397087	Hs.81131
19	1552474_a_	1,286	n	GAMT	19p13.3	19	1398451	Hs.81131
20	202638_s_a	-1,632	n	ICAM1	19p13.3-p1	19	10381778	Hs.643447
21	202637_s_a	-1,635	n	ICAM1	19p13.3-p1	19	10381763	Hs.643447
22	222240_s_a	-1,022	n	ISYNA1	19p13.11	19	18545631	Hs.724523
23	203751_x_a	1,010	n	JUND	19p13.2	19	18390570	Hs.2780
24	214326_x_a	-1,007	n	JUND	19p13.2	19	18391013	Hs.2780
26	213490_s_a	1,191	n	MAP2K2	19p13.3	7	128766471	Hs.465627
27	210075_at	-1,041	n	MARCH2	19p13.2	19	8486669	Hs.631861
30	203238_s_a	-1,380	n	NOTCH3	19p13.2-p1	19	15270444	Hs.8546
31	223601_at	-1,241	n	OLFM2	19p13.2	19	9964399	Hs.169743
32	203859_s_a	-1,394	n	PALM	19p13.3	19	709001	Hs.631841
37	34478_at	1,022	n	RAB11B	19p13.2	19	8454778	Hs.626404
38	203022_at	1,689	*	RNASEH2A	19p13.2	19	12917438	Hs.532851
39	213244_at	-1,058	n	SCAMP4	19p13.3	19	1925044	Hs.144980
40	235073_at	1,097	n	SCAMP4	19p13.3	19	1905405	Hs.144980
41	225175_s_a	1,535	**	SLC44A2	19p13.1	19	10754489	Hs.534560
42	216272_x_a	1,194	n	SYDE1	19p13.12	19	15223120	Hs.706845
43	212962_at	1,084	n	SYDE1	19p13.12	19	15220561	Hs.528701
44	216271_x_a	-1,077	n	SYDE1	19p13.12	19	15218244	Hs.528701
47	225655_at	2,404	**	UHRF1	19p13.3	12	20704503	Hs.108106
48	218110_at	-1,194	n	XAB2	19p13.2	19	7684411	Hs.9822

Row	UV vs. CON: RowNames	Fold Change	SIG	Gene.Symbol	pq	Chromosome	Physical.Position	UniGene.ID
9	208677_s_a	1,377	***	BSG	19p13.3	19	572564	Hs.501293
10	207722_s_a	1,251	n	BTBD2	19p13.3	19	1985446	Hs.465543
11	206399_x_a	1,054	n	CACNA1A	19p13.2-p1	19	13318114	Hs.501632
14	218975_at	-1,450	n	COL5A3	19p13.2	19	10070236	Hs.235368
15	201584_s_a	1,099	n	DDX39	19p13.12	19	14519626	Hs.311609
16	208255_s_a	1,065	n	FKBP8	19p12	19	18642572	Hs.173464
17	40850_at	1,131	n	FKBP8	19p12	19	18642572	Hs.173464
18	205354_at	2,035	****	GAMT	19p13.3	19	1397087	Hs.81131
19	1552474_a_	1,902	****	GAMT	19p13.3	19	1398451	Hs.81131
20	202638_s_a	1,553	*	ICAM1	19p13.3-p1	19	10381778	Hs.643447
21	202637_s_a	-1,035	n	ICAM1	19p13.3-p1	19	10381763	Hs.643447
22	222240_s_a	5,784	**	ISYNA1	19p13.11	19	18545631	Hs.724523
23	203751_x_a	1,690	****	JUND	19p13.2	19	18390570	Hs.2780
24	214326_x_a	1,907	****	JUND	19p13.2	19	18391013	Hs.2780
26	213490_s_a	1,163	n	MAP2K2	19p13.3	7	128766471	Hs.465627
27	210075_at	1,430	*	MARCH2	19p13.2	19	8486669	Hs.631861
30	203238_s_a	1,407	n	NOTCH3	19p13.2-p1	19	15270444	Hs.8546
31	223601_at	1,195	n	OLFM2	19p13.2	19	9964399	Hs.169743
32	203859_s_a	1,201	n	PALM	19p13.3	19	709001	Hs.631841
37	34478_at	1,176	n	RAB11B	19p13.2	19	8454778	Hs.626404
38	203022_at	-1,906	**	RNASEH2A	19p13.2	19	12917438	Hs.532851
39	213244_at	1,313	*	SCAMP4	19p13.3	19	1925044	Hs.144980
40	235073_at	1,296	n	SCAMP4	19p13.3	19	1905405	Hs.144980
41	225175_s_a	1,040	n	SLC44A2	19p13.1	19	10754489	Hs.534560
42	216272_x_a	1,010	n	SYDE1	19p13.12	19	15223120	Hs.706845
43	212962_at	-1,137	n	SYDE1	19p13.12	19	15220561	Hs.528701
44	216271_x_a	-1,320	n	SYDE1	19p13.12	19	15218244	Hs.528701
47	225655_at	-4,345	****	UHRF1	19p13.3	12	20704503	Hs.108106
48	218110_at	-1,439	*	XAB2	19p13.2	19	7684411	Hs.9822

Row	Gene.Title	Probe Set ID	UniGene ID	Alignment
9	basigin (Ok	208677_s_a	Hs.501293	chr19:57256
10	BTB (POZ) d	207722_s_a	Hs.465543	chr19:19854
11	calcium ch	206399_x_a	Hs.501632	chr19:13318
14	collagen, ty	218975_at	Hs.235368	chr19:10070
15	DEAD (Asp-	201584_s_a	Hs.311609	chr19:14519
16	FK506 bindi	208255_s_a	Hs.173464	chr19:18642
17	FK506 bindi	40850_at	Hs.173464	chr19:18642
18	guanidinoa	205354_at	Hs.81131	chr19:13970
19	guanidinoa	1552474_a_	Hs.81131	chr19:13984
20	intercellula	202638_s_a	Hs.643447	chr19:10381
21	intercellula	202637_s_a	Hs.643447	chr19:10381
22	inositol-3-pl	222240_s_a	Hs.724523	chr19:18545
23	jun D proto	203751_x_a	Hs.2780	chr19:18390
24	jun D proto	214326_x_a	Hs.2780	chr19:18391
26	mitogen-ac	213490_s_a	Hs.465627	chr7:128766
27	membrane	210075_at	Hs.631861	chr19:84866
30	Notch hom	203238_s_a	Hs.8546	chr19:15270
31	olfactomed	223601_at	Hs.169743	chr19:99643
32	paralemmi	203859_s_a	Hs.631841	chr19:70900
37	RAB11B, me	34478_at	Hs.626404	chr19:84547
38	ribonuclea	203022_at	Hs.532851	chr19:12917
39	secretory c	213244_at	Hs.144980	chr19:19250
40	secretory c	235073_at	Hs.144980	chr19:19054
41	solute carri	225175_s_a	Hs.534560	chr19:10754
42	synapse de	216272_x_a	Hs.706845	chr19:15223
43	synapse de	212962_at	Hs.528701	chr19:15220
44	synapse de	216271_x_a	Hs.528701	chr19:15218
47	ubiquitin-lik	225655_at	Hs.108106	chr12:20704
48	XPA bindin	218110_at	Hs.9822	chr19:76844

Supplementary Table 8. Regulation of telomeric 19p genes in normal and NBS fibroblasts with short telomeres (relative to cells with long telomeres).

Gene	Functions in senescence and/or cell growth	Reference	Distance to telomere [Mbp]	Differential gene expression, Affymetrix data	Differential gene expression, qPCR data Control fibroblasts	Differential gene expression, qPCR data NBS fibroblasts	TPE-OLD Effect
					[fold-change]		
BSG	MMP and cytokine production	[32]	0.6	+2.8	+3.2	+2.4	(N)
GAMT	ATP production (SASP?)	[33, 34]	1.4	+2.0	+5.6	+1.9	(N)
SCAMP4	player in SASP	[35]	1.9	+2.3	+1.9	+1.6	(N)
OLFM2	cell differentiation	[36]	9.9	+3.8	+50	+3.3	(N)
UHRF1	neg. regulator of senescence	[40]	4.9	-2.7	-5.0	+1.7	R
COL5A3	age-dependent tissue remodel.	[37]	10.0	+2.4	+25.0	+4.0	(N)
RNASEH2A	migration and invasion	[41]	12.8	-2.1	-4.5	+1.2	R
CACNA1A	calcium entry; nerve function	[38]	13.6	+2.1	+1.3	-1.5	R
DDX39A	role in cancer and longevity	[42]	14.6	-2.0	-2.2	+1.7	R
NOTCH3	pos. regulator of senescence (p21)	[39]	15.2	+4.1	+100.0	+58.0	(N)

BSG, basigin; GAMT, guanidinoacetate methyl-transferase; SCAMP4, secretory carrier membrane protein 4; OLFM2, olfactomedin 2; UHRF1, Ubiquitin like with PHD and ring finger domain 1; COL5A3, collagen type V alpha 3 chain; RNASEH2A, ribonuclease H2 subunit A; CACNA1A, calcium voltage-gated channel subunit alpha1 A; DDX39A, DExD-box helicase 39A; NOTCH3, Notch Receptor 3; SASP, senescence associated secretory phenotype; MMP, matrix metallopeptidases; (N), TPE-OLD: normal but attenuated regulation; R, TPE-OLD: reversed regulation, compared to regulation (mRNA) in healthy control fibroblasts; grey overlay: upregulation in pre-senescent cells; green overlay, down regulation in pre-senesecent cells

Supplementary Table 9. Correlation between telomere length and clinical data of 21 NBS homozygotes.

Telomere length	Age at cancer manifestation	Age at death
	p	p
Long vs.median	0.07	0.50
Median vs. short	0.52	0.54
Long vs. short	0.41	0.99

The p values are based on the unpaired T- test.